Chaos and the quantum phase transition in the Dicke model

Clive Emary* and Tobias Brandes
Department of Physics, UMIST, P.O. Box 88, Manchester M60 1QD, United Kingdom
(Received 15 January 2003; published 12 June 2003)

We investigate the quantum-chaotic properties of the Dicke Hamiltonian; a quantum-optical model that describes a single-mode bosonic field interacting with an ensemble of N two-level atoms. This model exhibits a zero-temperature quantum phase transition in the $N\to\infty$ limit, which we describe exactly in an effective Hamiltonian approach. We then numerically investigate the system at finite N, and by analyzing the level statistics, we demonstrate that the system undergoes a transition from quasi-integrability to quantum chaotic, and that this transition is caused by the precursors of the quantum phase transition. Our considerations of the wave function indicate that this is connected with a delocalization of the system and the emergence of macroscopic coherence. We also derive a semiclassical Dicke model that exhibits analogues of all the important features of the quantum model, such as the phase transition and the concurrent onset of chaos.

DOI: 10.1103/PhysRevE.67.066203 PACS number(s): 05.45.Mt, 42.50.Fx, 73.43.Nq

I. INTRODUCTION

Chaos plays a key role in considerations concerning the boundary between the classical and quantum worlds, not just because of the importance of chaos in classical physics [1], but because there is no direct analog of chaos in quantum mechanics [2]. The linearity of quantum dynamics precludes the characteristic exponential sensitivity to initial conditions of classical chaos, and forces us to look for what are known as ''signatures of quantum chaos''—properties whose presence in the quantum system would lead us to expect the corresponding classical motion to be chaotic [3]. Several such signatures have been identified, such as level statistics [4,5], level dynamics [6], and sensitivity to initial perturbation [7].

An often encountered feature of quantum-chaotic systems is that as some parameter is varied, these signatures bespeak a crossover from integrable to quantum-chaotic behavior. This parameter may, for example, describe the character of boundary conditions, such as the shape of a quantum billiard [5], the distribution of random fluctuations in disorder models [8–11], or the strength of some nonlinear potential or interaction [12–17]. A large class of models may be described by a Hamiltonian of the form

$$H=H_0+\lambda V, \tag{1}$$

where although H_0 is integrable, the full Hamiltonian H is not for any $\lambda\neq 0$. Here, increasing the parameter λ from zero upwards gradually drives the system away from integrability and towards chaos. A well studied, albeit time-dependent, example is the kicked rotator [3], where the parameter λ is the kick strength.

In this paper, we consider a system of the type described by Hamiltonian (1), but unlike the typically one-dimensional or noninteracting models, we shall consider a system of N *interacting* particles, in a situation where many-body and collective effects are critical. Specifically, the model we study exhibits a quantum phase transition (i.e., one at zero temperature [18]) in the thermodynamic limit of $N\to\infty$ at a critical value of the parameter, λ_c.

The influence of a quantum phase transition (QPT) on the transition to chaos has been studied in a handful of cases. Important examples include the three-dimensional Anderson model, where the metal-insulator transition is accompanied by a change in the level statistics [8], and models of spin glass shards [10], which have found topical application in the study of the effects of quantum chaos on quantum computing [11]. Heiss and co-workers have investigated the connection between the onset of chaos near a QPT and the exceptional points of the spectrum [19], both generically, and for the specific example of the Lipkin model [20].

In order to investigate the impact of QPT on the signatures of quantum chaos, we study the Dicke Hamiltonian (DH) [21], which is of key importance as a model describing the collective effects in quantum optics [22,23]. We demonstrate that there is a clear connection between the precursors of the QPT and the onset of quantum chaos as manifested in the level statistics. We are able to understand this connection by studying the wave functions of the system, and by deriving a semiclassical analog of this intrinsically quantum system. This paper is an extension of our previous work [24].

In the form considered here, the DH describes a collection of N two-level atoms interacting with a single bosonic mode via a dipole interaction with an atom-field coupling strength λ. The DH may be written as

$$H=\hbar\omega_0 J_z+\hbar\omega a^\dagger a+\frac{\lambda}{\sqrt{2j}}(a^\dagger+a)(J_++J_-), \tag{2}$$

where a, $a^\dagger$ describe a bosonic mode of frequency ω, and the angular momentum operators $\{J_i;\ i=z,\pm\}$ describe the ensemble of two-level atoms of level-splitting ω_0 in terms of a pseudospin of length $j=N/2$. The thermodynamic limit of $N\to\infty$ is thus equivalent to making the length of the pseudospin tend to infinity $j\to\infty$. The DH is usually considered in the standard quantum optics approach of the rotating-wave approximation (RWA), which is valid for small values of the

*Email address: emary@theory.phy.umist.ac.uk

coupling λ, and involves neglecting the counter-rotating terms $a^\dagger J_+$ and aJ_-. This makes the DH integrable, simplifying the analysis but also removing the possibility of quantum chaos. Dicke used this model to illustrate the importance of collective effects in the atom-light interaction [21], leading to the concept of super-radiance, where the atomic ensemble spontaneously emits with an intensity proportional to N^2 rather than N, as one would expect if the atoms were radiating incoherently [23].

The phase transition in the DH was first described by Hepp and Lieb [25], and a mathematically more transparent treatment was provided by Wang and Hioe [26]. They considered the thermodynamics of the model in the RWA, and concluded that for a coupling of $\lambda<\sqrt{\omega\omega_0}$ no phase transition occurs for any temperature, whereas for $\lambda>\sqrt{\omega\omega_0}$ there exists a critical temperature T_c given by

$$\frac{1}{k_B T_c}=\frac{2\omega}{\omega_0}\operatorname{arctanh}\left(\frac{\omega\omega_0}{\lambda^2}\right), \tag{3}$$

at which point the system undergoes a phase transition. Above the critical temperature, the system is in the effectively unexcited ''normal phase,'' whereas for $T<T_c$ the system is in the ''super-radiant phase,'' a macroscopically excited and highly collective state that possesses the potential to super-radiate.

In contrast to this earlier work, we shall consider this phase transition at zero temperature, where increasing the coupling λ through a critical value of $\lambda_c=\sqrt{\omega\omega_0}/2$ drives the system to undergo a transition from the normal to the super-radiant phase (the difference between this critical coupling λ_c and the value quoted for the finite-temperature case arises because the latter has been derived in the RWA, which renormalizes the critical coupling by a factor of 2 [27,28]). Here, we derive exact results without the RWA for the energy spectrum and eigenfunctions in the thermodynamic limit by employing a bosonization technique based upon the Holstein-Primakoff transformation of the angular momentum algebra [29,30]. This enables us to derive an effective Hamiltonian to describe the system in each of its two phases. One important step that we take is the introduction of an abstract position-momentum representation for both field and atomic systems. This not only facilitates the formulation of the exact solutions, but also provides us with a useful way of visualizing the wave functions across the phase transition. There is a discrete ''parity'' symmetry associated with this model, and at the phase transition this symmetry becomes broken. This QPT has been discussed in the RWA by Hillery and Mlodinow [31], using an effective Hamiltonian method that is similar to ours. However, having illustrated the existence of the QPT, they concentrated solely on the normal phase, and were not interested in chaos.

Away from the thermodynamic limit at finite N and j, the DH is, in general, nonintegrable. Quantum-chaotic properties of the DH have been discussed by several authors [32–39] but, to the best of our knowledge, have never been connected with the QPT, and a systematic study of the dependence of the systems behavior on the number of atoms N is lacking. Graham and Höhnerbach have contributed extensively to the discussion [32], especially in relation to the special case of spin-1/2 (the Rabi Hamiltonian), and have outlined many semiclassical and approximate schemes for these systems. Moreover, they have provided a preliminary analysis of the level statistics of the DH, concluding that spectra of the type associated with quantum chaos do occur for certain, isolated parameter values [33]. Several authors have conducted studies on chaos in various (semi)classical models related to DH [36–39]. That there have been several different semiclassical models is a consequence of the ambiguity in describing quantum spins in classical terms. The influence of the QPT also seems to have been overlooked in these semiclassical models.

We consider the quantum-mechanical system away from the thermodynamic limit by using numerical diagonalization, and examine the energy spectra of the system for signatures of quantum chaos. We consider the nearest-neighbor level-spacing distribution function $P(S)$, which is perhaps the best-known signature of quantum chaos [3]. We calculate the $P(S)$ for various values of N and λ and demonstrate a clear connection between the change in $P(S)$ from quasiintegrable to quantum chaotic and the coupling at which the QPT occurs, λ_c. We then proceed to consider the wave functions of the system at finite N using an abstract position-momentum representation. This enables us to conclude that the precursors of the QPT give rise to a localization-delocalization transition in which the ground-state wave function bifurcates into a macroscopic superposition for any $N<\infty$.

As mentioned above, much work has been done in trying to find a semiclassical analog of the DH [36–39]. The bosonization procedure that we employ here allows us to write the DH in terms of a pair of coupled harmonic oscillators. This suggests a very natural semiclassical analog of the DH, obtained by simply replacing the quantum oscillators with classical ones. We demonstrate that our semiclassical model reflects the quantum behavior better than those of previous studies. Specifically, our semiclassical model exhibits a symmetry-breaking phase transition in the limit that $N\to\infty$, and we show that the precursors of this classical transition give rise to the onset of classical chaos, in close agreement with the quantum model. An analog of the macroscopic superposition is also evident. In our conclusions, we pay special attention to the meaning of a classical limit for the DH and, in particular, the relevance of the semiclassical model derived here.

The paper is organized as follows. In Sec. II, we introduce the DH fully. Exact solutions are derived in the thermodynamic limit in Sec. III. Section IV sees an analysis of the level statistics and wave functions of the system at finite j. Our semiclassical model is derived in Sec. V, and its phase transition and chaotic properties are discussed. We discuss briefly the differences between the full DH and the Hamiltonian in the RWA in Sec. VI before we draw our final conclusions in Sec. VII. Some of our exact expressions are reproduced in the Appendix.

II. THE DICKE HAMILTONIAN

The full Dicke Hamiltonian (DH) models the interaction of N atoms with a number of bosonic field modes via dipole

interactions within an ideal cavity [21]. We initially represent the atoms as a collection of N identical, but distinguishable, two-level systems each with level splitting ω_0. The ith atom is described by the spin-1/2 operators $\{s_k^{(i)};\ k=z,\pm\}$, obeying the commutation rules $[s_z,s_\pm]=\pm s_\pm$; $[s_+,s_-]=2s_z$. These two-level atoms interact with M bosonic modes, which have frequencies $\{\omega_\alpha\}$, interact with coupling strengths $\{\lambda_\alpha\}$, and are described by the bosonic creation and annihilation operators $\{a_\alpha^\dagger\}$ and $\{a_\alpha\}$. In terms of these quantities, the full DH is given by

$$H=\omega_0\sum_{i=1}^{N}s_z^{(i)}+\sum_{\alpha=1}^{M}\omega_\alpha a_\alpha^\dagger a_\alpha + \sum_{\alpha=1}^{M}\sum_{i=1}^{N}\frac{\lambda_\alpha}{\sqrt{N}}(a_\alpha^\dagger+a_\alpha)(s_+^{(i)}+s_-^{(i)}), \tag{4}$$

where we have set $\hbar=1$. The origin of the factor $1/\sqrt{N}$ in the interaction is the fact that the original dipole coupling strength is proportional to $1/\sqrt{V}$, where V is the volume of the cavity. By writing $\rho=N/V$, where ρ is the density of the atoms in the cavity, this becomes $\sqrt{\rho/N}$ and by subsuming the density into the coupling constants $\{\lambda_\alpha\}$, we obtain $1/\sqrt{N}$ explicitly in the coupling.

In Eq. (4), we have not made the usual RWA under which one would neglect the counter-rotating terms $a_\alpha^\dagger s_+^{(i)}$ and $a_\alpha s_-^{(i)}$. We shall consider aspects of the RWA in Sec. VI.

We now specialize the Hamiltonian to consider a single-mode bosonic field, and thus we drop the subscript α. The analysis of this Hamiltonian is further simplified by the introduction of collective atomic operators

$$J_z\equiv\sum_{i=1}^{N}s_z^{(i)};\quad J_\pm\equiv\sum_{i=1}^{N}s_\pm^{(i)}. \tag{5}$$

These operators obey the usual angular momentum commutation relations

$$[J_z,J_\pm]=\pm J_\pm;\quad [J_+,J_-]=2J_z. \tag{6}$$

The Hilbert space of this algebra is spanned by the kets $\{|j,m\rangle;\ m=-j,-j+1,\ldots,j-1,j\}$, which are known as the Dicke states, and are eigenstates of J^2 and J_z: $J_z|j,m\rangle=m|j,m\rangle$ and $J^2|j,m\rangle=j(j+1)|j,m\rangle$. The raising and lowering operators act on these states in the following way: $J_\pm|j,m\rangle=\sqrt{j(j+1)-m(m\pm1)}\ |j,m\pm1\rangle$. Note that j corresponds to Dicke's "cooperation number," which takes the values $\frac{1}{2},\frac{3}{2},\ldots,N/2$ for N odd, and 0,1, . . . ,$N/2$ for N even. For example, with $N=2$ atoms, j can take the values 0 and 1. In terms of the s_z values of the individual spins, the sector with $j=1$ contains the triplet states $|\downarrow\downarrow\rangle$, $2^{-1/2}(|\uparrow\downarrow\rangle+|\downarrow\uparrow\rangle)$, and $|\uparrow\uparrow\rangle$. The $j=0$ sector contains only the singlet state $2^{-1/2}(|\uparrow\downarrow\rangle-|\downarrow\uparrow\rangle)$. In general, the set of atomic configurations for $N>2$ is nontrivial [40] and, in terms of the individual atom configurations, the states are nonseparable and contain entanglement [41]. In this work, we shall take j to have its maximal value $j=N/2$, and once set, this value of j is constant, since the interaction in the DH does not mix j sectors. Thus, the collection of N two-level systems is described as a single $(N+1)$-level system, which is viewed as a large pseudospin vector of length $j=N/2$.

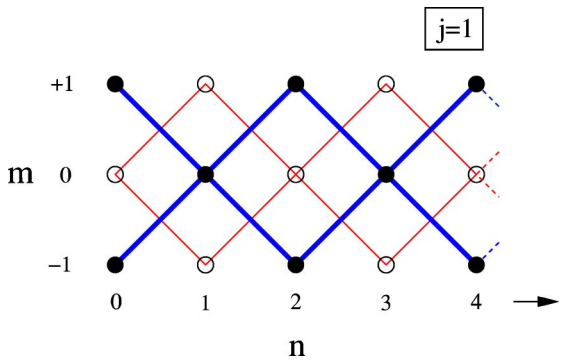

FIG. 1. Schematic lattice representation of the states of the Dicke model with $j=1$. Shaded (unshaded) dots denote states of positive (negative) parity, with solid lines representing the couplings between the states.

In terms of the collective operators, the single-mode DH may be written as

$$H=\omega_0 J_z+\omega a^\dagger a+\frac{\lambda}{\sqrt{2j}}(a^\dagger+a)(J_++J_-). \tag{7}$$

In the following, when we refer to the Dicke Hamiltonian we shall mean the single-mode Hamiltonian, unless otherwise stated. The resonance condition is $\omega=\omega_0$, and when plotting results we generally work on a scaled resonance, such that $\omega=\omega_0=1$.

Associated with the DH is a conserved parity Π, such that $[H,\Pi]=0$, which is given by

$$\Pi=\exp\{i\pi\hat{N}\},\quad \hat{N}=a^\dagger a+J_z+j, \tag{8}$$

where $\hat{N}$ is the "excitation number" and counts the total number of excitation quanta in the system. Π possesses two eigenvalues ±1, depending on whether the number of quanta is even or odd, and, correspondingly, the Hilbert space of the total system is split into two noninteracting subspaces.

If we express the Hilbert space of the total system in terms of the basis $\{|n\rangle\otimes|j,m\rangle\}$, where $|n\rangle$ are number states of the field, $a^\dagger a|n\rangle=n|n\rangle$, and $|j,m\rangle$ are the Dicke states, the DH and the significance of the parity operator may be viewed in a simple lattice analogy. We construct a two-dimensional lattice, each point of which represents a basis vector and is labeled (n,m). An example of this lattice with $j=1$ is shown in Fig. 1. Note that the lattice is finite in the "m" direction, but infinite in the 'n' direction, reflecting the dimensionality of the Hilbert space. In this picture, we see that because the interaction conserves the parity Π, states with an even total excitation number $n+m+j$ interact only with other even states, and odd states interact only with odd states. This has the effect of dividing the total lattice into two interweaved sublattices, which correspond to the two different parity sectors.

III. THERMODYNAMIC LIMIT

We begin by considering the DH in the thermodynamic limit, in which the number of atoms becomes infinite, $N\to\infty$, and hence $j\to\infty$. In this limit, the DH undergoes a QPT at a critical value of the atom-field coupling strength $\lambda_c=\sqrt{\omega\omega_0}/2$, at which point the symmetry associated with the parity operator Π of Eq. (8) is broken. To describe this QPT we shall derive two effective Hamiltonians, one to describe the system in the normal phase $\lambda<\lambda_c$ and one to describe it in the broken-symmetry, super-radiant phase $\lambda>\lambda_c$. It should be noted that the results derived below are exact in this limit, and this allows us to understand the nature of this system in a very detailed way.

In this analysis, we shall make an extensive use of the Holstein-Primakoff representation of the angular momentum operators, which represents the operators in terms of a single bosonic mode in the following way [29,30]:

$$J_+=b^\dagger\sqrt{2j-b^\dagger b},\quad J_-=\sqrt{2j-b^\dagger b}\;\; b,$$
$$J_z=(b^\dagger b-j), \tag{9}$$

where the introduced Bose operators obey $[b,b^\dagger]=1$.

Making these substitutions into the DH of Eq. (7), we obtain the two-mode bosonic Hamiltonian

$$H=\omega_0(b^\dagger b-j)+\omega a^\dagger a+\lambda(a^\dagger+a)\left(b^\dagger\sqrt{1-\frac{b^\dagger b}{2j}}+\sqrt{1-\frac{b^\dagger b}{2j}}b\right). \tag{10}$$

In this representation, the parity operator Π becomes

$$\Pi=\exp\{i\pi[a^\dagger a+b^\dagger b]\}, \tag{11}$$

and the analogy with the standard parity operator of a two-dimensional harmonic operator is thus apparent [42].

A. Normal phase

We derive an effective Hamiltonian for the system in the normal phase by simply neglecting terms with j in the denominator in the full Hamiltonian of Eq. (10). This approximates the square root in the Holstein-Primakoff mapping with unity, and we obtain the effective Hamiltonian $H^{(1)}$ given by

$$H^{(1)}=\omega_0 b^\dagger b+\omega a^\dagger a+\lambda(a^\dagger+a)(b^\dagger+b)-j\omega_0, \tag{12}$$

which is bilinear in the bosonic operators and can thus be simply diagonalized. This is most easily facilitated by the introduction of position and momentum operators for the two bosonic modes,

$$x=\frac{1}{\sqrt{2\omega}}(a^\dagger+a),\quad p_x=i\sqrt{\frac{\omega}{2}}(a^\dagger-a),$$
$$y=\frac{1}{\sqrt{2\omega_0}}(b^\dagger+b),\quad p_y=i\sqrt{\frac{\omega_0}{2}}(b^\dagger-b). \tag{13}$$

This representation will be particularly useful when we come to consider the wave functions of the system. Expressing the Hamiltonian $H^{(1)}$ in terms of these operators, we obtain

$$H^{(1)}=\frac{1}{2}\{\omega^2x^2+p_x^2+\omega_0^2y^2+p_y^2+4\lambda\sqrt{\omega\omega_0}\;\;xy-\omega_0-\omega\}-j\omega_0, \tag{14}$$

which may be diagonalized by rotating the coordinate system in the following way:

$$x=q_1\cos\gamma^{(1)}+q_2\sin\gamma^{(1)};\quad y=-q_1\sin\gamma^{(1)}+q_2\cos\gamma^{(1)}, \tag{15}$$

where the angle $\gamma^{(1)}$ is given by

$$\tan(2\gamma^{(1)})=\frac{4\lambda\sqrt{\omega\omega_0}}{\omega_0^2-\omega^2}. \tag{16}$$

On resonance, $\omega=\omega_0$, $\gamma^{(1)}=\pi/4$, so that $x=(q_1+q_2)/\sqrt{2}$ and $y=(-q_1+q_2)/\sqrt{2}$. This rotation eliminates the xy interaction term in the Hamiltonian, which then assumes the form of two uncoupled oscillators,

$$H^{(1)}=\frac{1}{2}\{\varepsilon_-^{(1)2}q_1^2+p_1^2+\varepsilon_+^{(1)2}q_2^2+p_2^2-\omega-\omega_0\}-j\omega_0. \tag{17}$$

We now requantize $H^{(1)}$ with the introduction of two new bosonic modes defined by

$$q_1=\frac{1}{\sqrt{2\varepsilon_-^{(1)}}}(c_1^\dagger+c_1),\quad p_1=i\sqrt{\frac{\varepsilon_-^{(1)}}{2}}(c_1^\dagger-c_1),$$
$$q_2=\frac{1}{\sqrt{2\varepsilon_+^{(1)}}}(c_2^\dagger+c_2),\quad p_2=i\sqrt{\frac{\varepsilon_+^{(1)}}{2}}(c_2^\dagger-c_2), \tag{18}$$

and arrive at the final diagonal form

$$H^{(1)}=\varepsilon_-^{(1)}c_1^\dagger c_1+\varepsilon_+^{(1)}c_2^\dagger c_2+\frac{1}{2}(\varepsilon_+^{(1)}+\varepsilon_-^{(1)}-\omega-\omega_0)-j\omega_0. \tag{19}$$

The bosonic operators $\{c_1,c_1^\dagger,c_2,c_2^\dagger\}$, in terms of which $H^{(1)}$ is diagonal, are linear combinations of the original operators $\{a,a^\dagger,b,b^\dagger\}$, as detailed in Appendix A, and describe collective atom-field excitations. The energies of the two independent oscillator modes $\varepsilon_\pm^{(1)}$ are given by

$$\varepsilon_\pm^{(1)2}=\frac{1}{2}\{\omega^2+\omega_0^2\pm\sqrt{(\omega_0^2-\omega^2)^2+16\lambda^2\omega\omega_0}\}. \tag{20}$$

Crucially, we see that the excitation energy $\varepsilon_-^{(1)}$ is real only when $\omega^2+\omega_0^2\geqslant\sqrt{(\omega_0^2-\omega^2)^2+16\lambda^2\omega\omega_0}$, or equivalently $\lambda\leqslant\sqrt{\omega\omega_0}/2=\lambda_c$. Thus, we see that $H^{(1)}$ remains valid for $\lambda\leqslant\lambda_c$, i.e., in the normal phase. In this phase, the ground-state energy is given by $E_G^{(1)}=-j\omega_0$, which is $O(j)$, whereas the excitation energies $\varepsilon_\pm^{(1)}$ are $O(1)$. This means

that by scaling our energies with j, the excitation spectrum above the ground state becomes quasicontinuous in the $j \to \infty$ limit; that is to say that the excitation energies differ by an infinitesimal amount from E_G.

It should be noted that $H^{(1)}$ commutes with the parity operator Π, and thus the eigenstates of $H^{(1)}$ have a definite parity, with the ground state having positive parity. This can been seen from the fact that at $\lambda = 0$, the ground state is $|0\rangle|j,-j\rangle$ in the original $|n\rangle|j,m\rangle$ basis, which clearly has an even excitation number, $n+m+j=0$. As the energy levels in the normal phase are nondegenerate, the continuity of the ground state with increasing λ ensures that it always has positive parity in this phase.

B. Super-radiant phase

In order to describe the system above the phase transition, we must incorporate the fact that both the field and the atomic ensemble acquire macroscopic occupations. To do this, we start with the Holstein-Primakoff transformed Hamiltonian of Eq. (10) and displace the bosonic modes in either of the following ways:

$$a^\dagger \to c^\dagger + \sqrt{\alpha}; \quad b^\dagger \to d^\dagger - \sqrt{\beta} \tag{21}$$

or

$$a^\dagger \to c^\dagger - \sqrt{\alpha}; \quad b^\dagger \to d^\dagger + \sqrt{\beta}. \tag{22}$$

Crucially, we assume that the as yet, undetermined parameters α and β are of the $O(j)$, equivalent to assuming that both modes acquire nonzero, macroscopic mean fields above λ_c. In the following, we shall just consider the displacements given by Eq. (21), as the calculation with the other choice is identical but for a few changes of sign.

Making these displacements, the Hamiltonian of Eq. (10) becomes

$$H = \omega_0\{d^\dagger d - \sqrt{\beta}(d^\dagger + d) + \beta - j\} + \omega\{c^\dagger c + \sqrt{\alpha}(c^\dagger + c) + \alpha\} + \lambda\sqrt{\frac{k}{2j}}(c^\dagger + c + 2\sqrt{\alpha})(d^\dagger\sqrt{\xi} + \sqrt{\xi}d - 2\sqrt{\beta}\sqrt{\xi}), \tag{23}$$

where for brevity we have written

$$\sqrt{\xi} \equiv \sqrt{1 - \frac{d^\dagger d - \sqrt{\beta}(d^\dagger + d)}{k}}$$

and $k \equiv 2j - \beta$. Taking the thermodynamic limit by expanding the square root $\sqrt{\xi}$ and then setting terms with overall powers of j in the denominator to zero, we obtain

$$H^{(2)} = \omega c^\dagger c + \left\{\omega_0 + \frac{2\lambda}{k}\sqrt{\frac{\alpha\beta k}{2j}}\right\} d^\dagger d - \left\{2\lambda\sqrt{\frac{\beta k}{2j}} - \omega\sqrt{\alpha}\right\} \times (c^\dagger + c) + \left\{\frac{4\lambda}{k}\sqrt{\frac{\alpha k}{2j}}(j-\beta) - \omega_0\sqrt{\beta}\right\}(d^\dagger + d) + \frac{\lambda}{2k^2}\sqrt{\frac{\alpha\beta k}{2j}}(2k+\beta)(d^\dagger + d)^2 + \frac{2\lambda}{k}\sqrt{\frac{k}{2j}}(j-\beta) \times (c^\dagger + c)(d^\dagger + d) + \left\{\omega_0(\beta - j) + \omega\alpha - \frac{\lambda}{k}\sqrt{\frac{\alpha\beta k}{2j}} \times (1+4k)\right\}. \tag{24}$$

We now eliminate the terms in the $H^{(2)}$ that are linear in the bosonic operators by choosing the displacements α and β so that

$$2\lambda\sqrt{\frac{\beta k}{2j}} - \omega\sqrt{\alpha} = 0 \tag{25}$$

and

$$\left\{\frac{4\lambda^2}{\omega j}(j-\beta) - \omega_0\right\}\sqrt{\beta} = 0. \tag{26}$$

The $\sqrt{\beta} = \sqrt{\alpha} = 0$ solution of these equations recovers the normal phase Hamiltonian $H^{(1)}$. The nontrivial solution gives

$$\sqrt{\alpha} = \frac{2\lambda}{\omega}\sqrt{\frac{j}{2}(1-\mu^2)}; \quad \sqrt{\beta} = \sqrt{j(1-\mu)}, \tag{27}$$

where we have defined

$$\mu \equiv \frac{\omega\omega_0}{4\lambda^2} = \frac{\lambda_c^2}{\lambda^2}. \tag{28}$$

With these determinations, the effective Hamiltonian of Eq. (24) becomes

$$H^{(2)} = \omega c^\dagger c + \frac{\omega_0}{2\mu}(1+\mu)d^\dagger d + \frac{\omega_0(1-\mu)(3+\mu)}{8\mu(1+\mu)}(d^\dagger + d)^2 + \lambda\mu\sqrt{\frac{2}{1+\mu}}(c^\dagger + c)(d^\dagger + d) - j\left\{\frac{2\lambda^2}{\omega} + \frac{\omega_0^2\omega}{8\lambda^2}\right\} - \frac{\lambda^2}{\omega}(1-\mu). \tag{29}$$

To facilitate the diagonalization of this bilinear Hamiltonian we move to a position-momentum representation defined by

$$X \equiv \frac{1}{\sqrt{2\omega}}(c^\dagger + c), \quad P_X \equiv i\sqrt{\frac{\omega}{2}}(c^\dagger - c);$$

$$Y \equiv \frac{1}{\sqrt{2\tilde{\omega}}}(d^\dagger + d), \quad P_Y \equiv i\sqrt{\frac{\tilde{\omega}}{2}}(d^\dagger - d), \tag{30}$$

where $\tilde{\omega} = (\omega_0/2\mu)(1+\mu)$. Note that this is not the same representation as defined in Eq. (13). The diagonalization then proceeds similarly as before, involving a rotation in the X-Y plane to the new coordinates

$$X = Q_1 \cos\gamma^{(2)} + Q_2 \sin\gamma^{(2)},$$

$$Y = -Q_1 \sin\gamma^{(2)} + Q_2 \cos\gamma^{(2)}, \tag{31}$$

with the angle $\gamma^{(2)}$ given by

$$\tan(2\gamma^{(2)}) = \frac{2\omega\omega_0\mu^2}{\omega_0^2 - \mu^2\omega^2}. \tag{32}$$

A subsequent requantization in terms of two new modes $e_\pm^{(2)}$, corresponding to the rotated, decoupled oscillators gives us the diagonal form

$$H^{(2)} = \varepsilon_-^{(2)} e_1^\dagger e_1 + \varepsilon_+^{(2)} e_2^\dagger e_2 - j\left\{\frac{2\lambda^2}{\omega} + \frac{\omega_0^2\omega}{8\lambda^2}\right\} + \frac{1}{2}\left(\varepsilon_+^{(2)} + \varepsilon_-^{(2)} - \frac{\omega_0}{2\mu}(1+\mu) - \omega - \frac{2\lambda^2}{\omega}(1-\mu)\right), \tag{33}$$

with the oscillator energies being given by

$$2\varepsilon_\pm^{(2)2} = \frac{\omega_0^2}{\mu^2} + \omega^2 \pm \sqrt{\left[\frac{\omega_0^2}{\mu^2} - \omega^2\right]^2 + 4\omega^2\omega_0^2}. \tag{34}$$

The Bogoliubov transformations that induce this diagonalization are given in Appendix A. The excitation energy $\varepsilon_-^{(2)}$, and hence $H^{(2)}$, remains real, provided that $(\omega_0^2/\mu^2) + \omega^2 \geq \sqrt{[(\omega_0^2/\mu^2) - \omega^2]^2 + 4\omega^2\omega_0^2}$ or, equivalently, $\lambda \geq \sqrt{\omega\omega_0}/2 = \lambda_c$. Thus, we see that $H^{(2)}$ describes the system in the super-radiant phase, $\lambda \geq \lambda_c$, in which the scaled ground-state energy is given by $E_G^{(2)}/j = -\{(2\lambda^2/\omega) + (\omega_0^2\omega/8\lambda^2)\}$.

If we choose the signs of the operator displacements as per Eq. (22), we obtain exactly the same values of α and β, and an effective Hamiltonian identical in form to Eq. (33), This clearly has the same spectrum and, therefore, each and every level of the total spectrum is doubly degenerate above the phase transition. What has occurred is that the symmetry of the ground state, defined by the operator Π, has become spontaneously broken at λ_c. The Hamiltonian $H^{(2)}$, for either choice of displacement, does not commute with Π, and thus its eigenfunctions do not possess good parity symmetry.

Although the global symmetry Π becomes broken at the phase transition, two new local symmetries appear, corresponding to the operator

$$\Pi^{(2)} \equiv \exp\{i\pi[c^\dagger c + d^\dagger d]\} \tag{35}$$

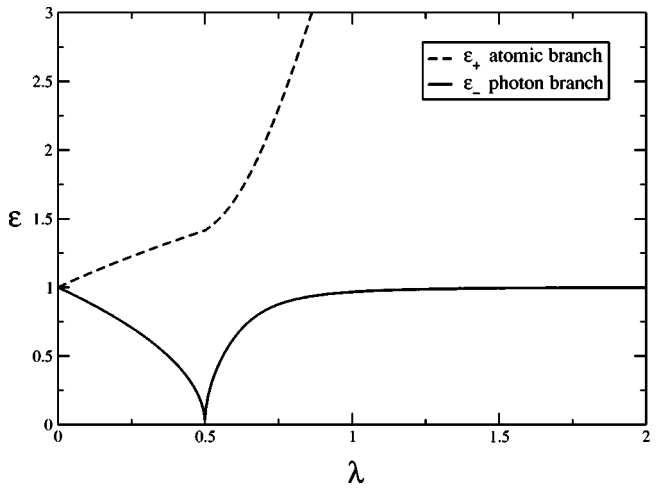

FIG. 2. The excitation energies of the Dicke Hamiltonian in the thermodynamic limit as a function of coupling λ. The Hamiltonian is on scaled resonance, $\omega = \omega_0 = 1$, and the vanishing of ε_- at $\lambda = \lambda_c = 0.5$ signals the occurrence of the QPT.

for both of the two different choices of mean-field displacements. This operator commutes with the appropriate super-radiant Hamiltonian $[H^{(2)}, \Pi^{(2)}] = 0$.

C. Phase transition

Having derived the two effective Hamiltonians that describe the system for all λ in the $j \to \infty$ limit, we now describe the system's properties in each of its two phases. The fundamental excitations of the system are given by the energies $\varepsilon_\pm$, which describe collective modes, similar to polariton modes in solid-state physics [43]. The behavior of these energies as a function of coupling strength is displayed in Fig. 2, where we have labeled the two branches as ''atomic'' and ''photonic,'' according to the nature of the excitation at zero coupling. From this figure we see that as the coupling approaches the critical value λ_c, the excitation energy of the photonic mode vanishes, $\varepsilon_- \to 0$, as $\lambda \to \lambda_c$, demonstrating the existence of the QPT. In contrast, ε_+ tends towards a value of $\sqrt{\omega_0^2 + \omega^2}$ as $\lambda \to \lambda_c$ from either direction. In the asymptotic limit of $\lambda \to \infty$, $\varepsilon_- \to \omega$ (returning to its $\lambda = 0$ value), whereas $\varepsilon_+ \to 4\lambda^2/\omega$. The critical exponents of this QPT are manifested in the behavior of the excitation energies [18]. As $\lambda \to \lambda_c$ from either direction, the energy ε_- can be shown to vanish as

$$\varepsilon_-(\lambda \to \lambda_c) \sim \sqrt{\frac{32\lambda_c^3\omega^2}{16\lambda_c^4 + \omega^4}}|\lambda_c - \lambda|^{1/2}. \tag{36}$$

The vanishing of ε_- at λ_c reveals this to be a second-order phase transition. We define the characteristic length scale in the system in terms of this energy as

$$l_- = 1/\sqrt{\varepsilon_-}\,. \tag{37}$$

From Eq. (36), this length diverges as $|\lambda - \lambda_c|^{-\nu}$ with the exponent $\nu = 1/4$. We then write that ε_- vanishes as

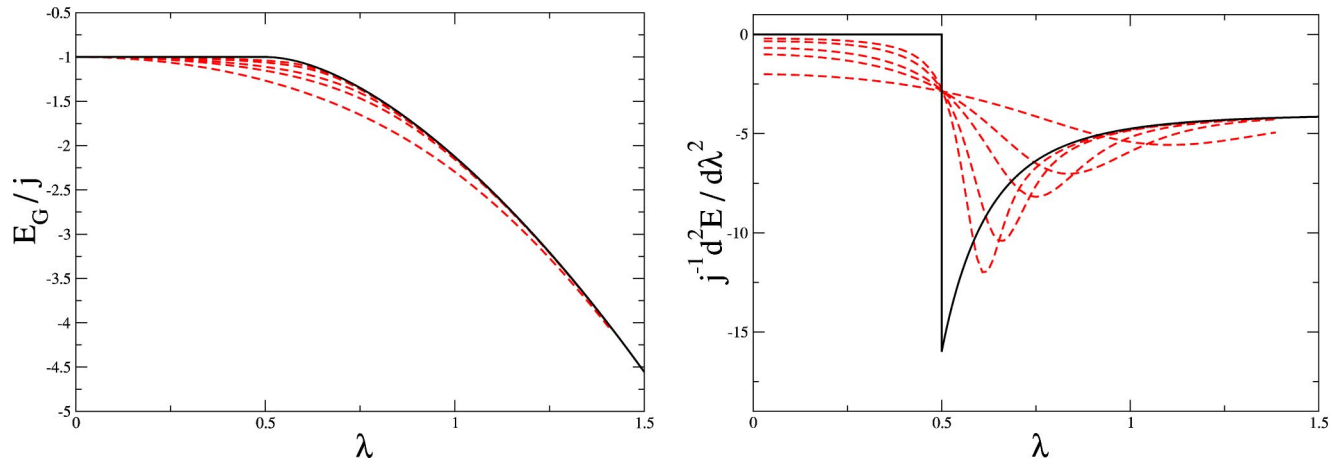

FIG. 3. The scaled ground-state energy E_G/j and its second derivative $j^{-1}d^2E_G/d\lambda^2$ as a function of coupling λ. Solid lines denote results in the thermodynamic limit, whereas dashed lines correspond to the results for various finite values of $j=\frac{1}{2},1,\frac{3}{2},3,5$. The Hamiltonian is on scaled resonance: $\omega=\omega_0=1$, $\lambda_c=0.5$.

$|\lambda-\lambda_c|^{z\nu}$, with the dynamical critical exponent being given by $z=2$. At the phase transition point, we have

$$H^{(1)}(\lambda_c)=H^{(2)}(\lambda_c)$$
$$=\sqrt{\omega^2+\omega_0^2}c_2^\dagger c_2+\frac{1}{2}(\sqrt{\omega^2+\omega_0^2}-\omega-\omega_0)-j\omega_0, \tag{38}$$

from which we see that at λ_c the system becomes effectively one dimensional.

The ground-state energy of the system E_G is shown in Fig. 3 and the analytic form expression is given in Table I. Note that we scale all quantities by j, which means that the plotted E_G/j is equal to $2E_G/N$, twice the energy per atom. We also plot the second derivative of the ground-state energy with respect to λ, which possesses a discontinuity at λ_c, clearly locating the phase transition.

In Fig. 4, we plot the atomic inversion $\langle J_z\rangle/j$ and the mean photon number $\langle n_a\rangle/j\equiv\langle a^\dagger a\rangle/j$. This figure clearly illustrates the nature of the phase transition; in the normal phase, the system is only microscopically excited, whereas above λ_c both the field and the atomic ensemble acquire macroscopic excitations. We may write the values of the atomic inversion and the mean photon number above λ_c in the following fashion:

$$\langle J_z\rangle/j=\beta/j-1, \quad \langle a^\dagger a\rangle/j=\alpha/j; \quad \lambda>\lambda_c. \tag{39}$$

Thus, making clear the physical meaning of the displacement parameters α and β in Eqs. (27).

D. Ground-state wave function

We now consider the ground-state wave functions of the system above and below the phase transition. After diagonalization, the two effective Hamiltonians are both of the form of a pair of uncoupled harmonic oscillators. Thus, in the representation in which the Hamiltonians are diagonal, their wave functions will simply be the product of the appropriate harmonic oscillator eigenfunctions. Here, we seek to express

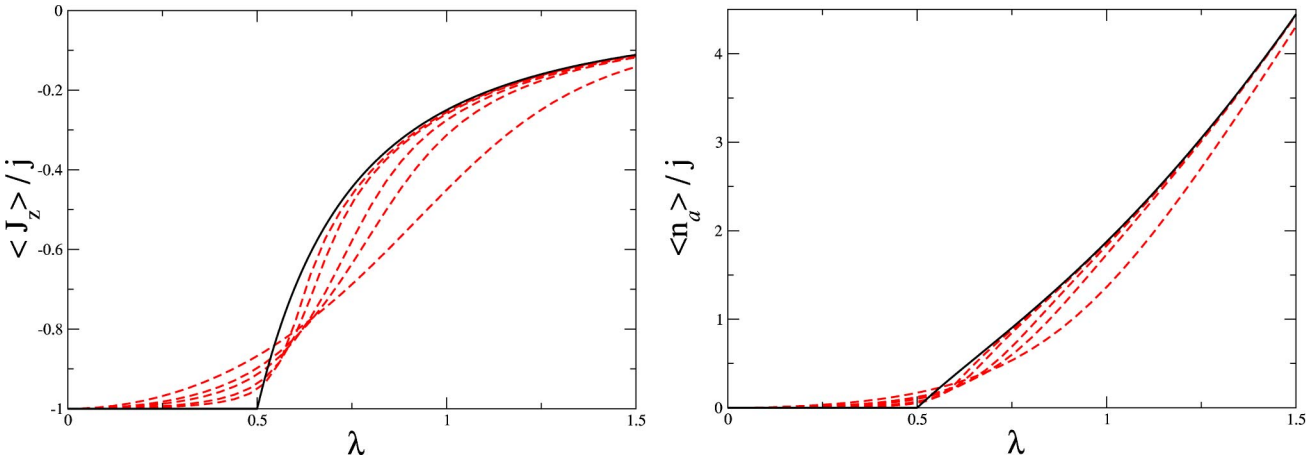

FIG. 4. The scaled atomic inversion and the mean photon number of the Dicke Hamiltonian as a function of coupling λ. Solid lines denote results in the thermodynamic limit, whereas dashed lines correspond to the results for various finite values of $j=\frac{1}{2},1,\frac{3}{2},3,5$. The Hamiltonian is on scaled resonance: $\omega=\omega_0=1$, $\lambda_c=0.5$.

TABLE I. The ground-state energy, atomic inversion, and mean photon number of the Dicke Hamiltonian in the thermodynamic limit.

	$\lambda<\lambda_c$	$\lambda>\lambda_c$
E_G/j	$-\omega_0$	$-\frac{2\lambda^2}{\omega}-\frac{2\lambda_c^4}{\lambda^2\omega}$
$\langle J_z\rangle/j$	-1	$-\lambda_c^2/\lambda^2$
$\langle a^\dagger a\rangle/j$	0	$2(\lambda^4-\lambda_c^4)/(\omega\lambda)^2$

these wave functions in terms of the two-dimensional x-y representation of Eq. (13)—which corresponds to the original atomic and field degrees of freedom.

We have already noted that in the Holstein-Primakoff representation, the parity operator has the form $\Pi=\exp\{i\pi[a^\dagger a+b^\dagger b]\}$. From our knowledge of the harmonic oscillator [42], we know that the action of Π in the x-y representation is to perform the coordinate inversions, $x\rightarrow -x$ and $y\rightarrow -y$, with p_x and p_y remaining unaffected. Thus, the operation of Π is equivalent to a rotation of π about the coordinate origin and, in the normal phase where Π is a good quantum number, the wave functions will be seen to be invariant under this rotation.

The ground-state wave function of a single harmonic oscillator in terms of its coordinate q is a Gaussian with width determined by the energy of the oscillator. Correspondingly, we define the normalized Gaussian functions

$$G_{\pm}^{(1,2)}(q)=\left(\frac{\varepsilon_{\pm}^{(1,2)}}{\pi}\right)^{1/4}\exp\left\{-\frac{\varepsilon_{\pm}^{(1,2)}}{2}q^2\right\}, \tag{40}$$

where $\varepsilon_{\pm}^{(1,2)}$ are the excitation energies encountered earlier.

In the normal phase, the effective Hamiltonian $H^{(1)}$ is diagonal in the q_1-q_2 representation of Eq. (15) and its ground-state wave function $\Psi_G^{(1)}$ in this representation is, therefore,

$$\Psi_G^{(1)}(q_1,q_2)=G_-^{(1)}(q_1)G_+^{(1)}(q_2). \tag{41}$$

Moving to the x-y representation, we have

$$\Psi_G^{(1)}(x,y)=G_-^{(1)}(x\cos\gamma^{(1)}-y\sin\gamma^{(1)})\times G_+^{(1)}(x\sin\gamma^{(1)}+y\cos\gamma^{(1)}), \tag{42}$$

and this wave function is plotted for various couplings in Fig. 5. At $\lambda=0$, the wave function is the product of orthogonal Gaussians of equal width (on resonance). As coupling increases, the wave packet becomes stretched in a direction determined by the angle $\gamma^{(1)}$ that on resonance is simply equal to $\pi/4$. This stretching increases up to λ_c, where the wave function diverges. We thus see the significance of the length l_- introduced earlier—it is the extent of the wave function in the direction of this stretching. Correspondingly, l_+ is the extent of the wave function in the orthogonal direction.

In the super-radiant phase, the ground state is degenerate. We shall initially consider the ground-state wave function of the effective Hamiltonian $H^{(2)}$ with displacements chosen in Eq. (21). This is diagonal in the Q_1-Q_2 representation of Eq. (31), and therefore its ground-state wave function is

$$\Psi_G^{(2)}(Q_1,Q_2)=G_-^{(2)}(Q_1)G_+^{(2)}(Q_2). \tag{43}$$

Using Eqs. (13), (21), (30), and (31) we may write this in the original x-y representation as

$$\Psi_G^{(2)}(x,y)=G_-^{(2)}[(x-\sqrt{2\alpha/\omega})\cos\gamma^{(2)}-\sqrt{\omega_0/\tilde{\omega}}\times(y+\sqrt{2\beta/\omega_0})\sin\gamma^{(2)}]G_+^{(2)}[(x-\sqrt{2\alpha/\omega})\times\sin\gamma^{(2)}+\sqrt{\omega_0/\tilde{\omega}}(y+\sqrt{2\beta/\omega_0})\cos\gamma^{(2)}]. \tag{44}$$

This expression contains displacements involving the macroscopic quantities α and β, and so we define the new coordinates x' and y' to remove them:

$$x'\equiv x-\Delta_x,\quad y'\equiv y+\Delta_y, \tag{45}$$

with

$$\Delta_x\equiv\sqrt{2\alpha/\omega},\quad \Delta_y\equiv\sqrt{2\beta/\omega_0}, \tag{46}$$

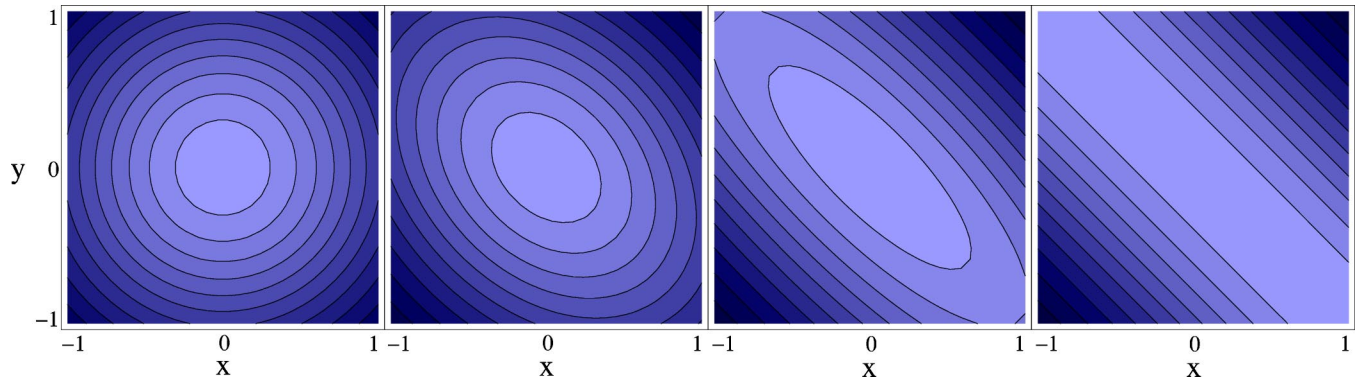

FIG. 5. The ground-state wave function $\Psi_G^{(1)}$ of the low-coupling Hamiltonian $H^{(1)}$ in the x-y position-momentum representation for couplings $\lambda=0,0.3,0.49,0.499\,999\,9$. The Hamiltonian is on scaled resonance: $\omega=\omega_0=1$, $\lambda_c=0.5$.

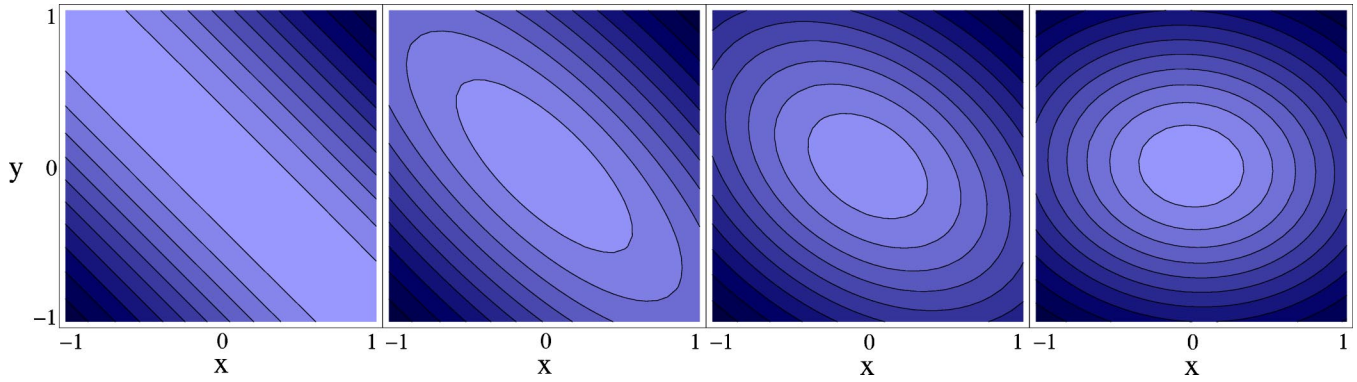

FIG. 6. The ground-state wave function $\Psi_G^{(2)}$ of the high-coupling Hamiltonian $H^{(2)}$ in the x'-y' position-momentum representation for couplings $\lambda = 0.500\,001, 0.51, 0.6, 1.0$. The Hamiltonian is on scaled resonance: $\omega = \omega_0 = 1$, $\lambda_c = 0.5$.

which are both proportional to $\sqrt{j}$. The relationship between the coordinate system X-Y of Eq. (30) and x'-y' is very simple, namely, $x' = X$ and $y' = \sqrt{\tilde{\omega}/\omega_0}\, Y$. The coordinate system x'-y' is useful because although X-Y is the diagonal representation for the super-radiant phase, the definition of these coordinates depends upon $\tilde{\omega}$ and hence upon λ, which distorts the picture. In terms of these coordinates, the wave function becomes

$$\Psi_G^{(2)}(x',y') = (\omega_0/\tilde{\omega})^{1/4} G_-^{(2)}(x' \cos\gamma^{(2)} - \sqrt{\omega_0/\tilde{\omega}}\, y' \sin\gamma^{(2)}) G_+^{(2)}(x' \sin\gamma^{(2)} + \sqrt{\omega_0/\tilde{\omega}}\, y' \cos\gamma^{(2)}). \quad (47)$$

Figure 6 shows $\Psi_G^{(2)}(x',y')$ for four different couplings. Just above the phase transition the wave function is in a highly deformed state, characterized by the divergent l_-. As the coupling increases further above λ_c, the wave function relaxes back to a well localized state.

When considered in the original x-y representation, the wave function $\Psi_G^{(2)}(x',y')$ pictured in Fig. 6 is centered about the point $(+\Delta_x, -\Delta_y)$, which lies in the lower-right quadrant of the x-y plane. The complementary wave function, identical in shape with this one but determined by displacements (22), is centered at $(-\Delta_x, +\Delta_y)$ in the upper-left quadrant. The positions of these two centers as parametric functions of coupling are shown in Fig. 7. These two wave functions, corresponding to the two choices of displacement, are separated from the origin by an amount proportional to $\sqrt{j}$. It is thus clear that neither of these wave functions is symmetric under rotation of π about the origin of the x-y coordinate system, demonstrating once more that the Π symmetry has been broken. There is, however, symmetry with respect to a rotation of π about the origin of each $x'-y'$ coordinate system, which corresponds to the existence of the local symmetries associated with $\Pi^{(2)}$ of Eq. (35).

It is interesting to consider the behavior of the ground-state wave function as $\lambda \to \infty$. In this limit $\varepsilon_-^{(2)} \to \omega$, $\varepsilon_+^{(2)} \to 4\lambda^2/\omega$ and the mixing angle of the two modes $\gamma^{(2)}$ tends to zero, meaning that the modes decouple. The Bogoliubov transformations of the modes become

$$e_1^\dagger \to c^\dagger, \quad e_1 \to c,$$

$$e_2^\dagger \to \frac{1}{2\sqrt{2}}(3d^\dagger + d), \quad e_2 \to \frac{1}{2\sqrt{2}}(d^\dagger + 3d), \quad (48)$$

illustrating the decoupling. Note that the e_1 simply reverts to the c mode, whereas the e_2 mode tends towards a linear combination of the annihilation and creation operators. In this limit, the wave function becomes

$$\Psi_G^{(2)}(x',y') \to \left(\frac{\omega\omega_0}{2\lambda^2}\right)^{1/4} G_-^{(2)}(x') G_+^{(2)}\left(\frac{\sqrt{2}\lambda_c}{\lambda} y'\right) = \sqrt{\frac{2\lambda_c}{\pi}} \exp\left(-\omega_0 y'^2 - \frac{\omega}{2} x'^2\right), \quad (49)$$

which is independent of λ.

E. Squeezing

A bosonic field may said to be squeezed if the uncertainty in either of its quadratures (x or p_x) is less than the uncertainty in a coherent state [44]. A coherent state is a minimum

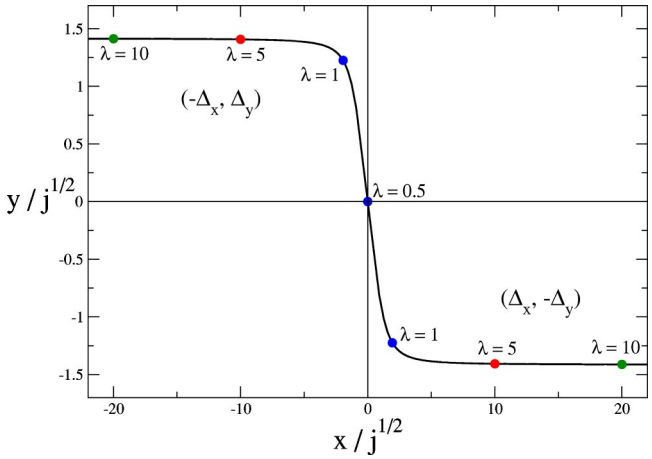

FIG. 7. Parametric plot of the (scaled) displacements $(\Delta_x, -\Delta_y)$ and $-(\Delta_x, \Delta_y)$ as λ is varied between 0.5 and 10. The Hamiltonian is on scaled resonance; $\omega = \omega_0 = 1$.

uncertainty state with $(\Delta x)^2(\Delta p_x)^2=1/4$ and with the uncertainty apportioned evenly between the two quadratures. Therefore, the field is squeezed whenever $(\Delta x)^2$ or $(\Delta p_x)^2$ has a value lower than 1/2 [45].

We define the two quadrature variances of the original field mode a by $(\Delta x)^2\equiv\langle x^2\rangle-\langle x\rangle^2$ and $(\Delta p_x)^2\equiv\langle p_x^2\rangle-\langle p_x\rangle^2$, which may be seen to be equal to

$$(\Delta x)^2=\frac{1}{2\omega}\{1+\langle a^{\dagger 2}\rangle+\langle a^2\rangle+2\langle a^\dagger a\rangle+(\langle a^\dagger\rangle+\langle a\rangle)^2\},$$

$$(\Delta p_x)^2=\frac{\omega}{2}\{1-\langle a^{\dagger 2}\rangle-\langle a^2\rangle+2\langle a^\dagger a\rangle+(\langle a^\dagger\rangle+\langle a\rangle)^2\}. \tag{50}$$

As we have introduced a bosonic algebra for the atomic collection, we now introduce an analogous definition for squeezing in the atoms, and say that in terms of the variances

$$(\Delta y)^2=\frac{1}{2\omega_0}\{1+\langle b^{\dagger 2}\rangle+\langle b^2\rangle+2\langle b^\dagger b\rangle+(\langle b^\dagger\rangle+\langle b\rangle)^2\},$$

$$(\Delta p_y)^2=\frac{\omega_0}{2}\{1-\langle b^{\dagger 2}\rangle-\langle b^2\rangle+2\langle b^\dagger b\rangle+(\langle b^\dagger\rangle+\langle b\rangle)^2\}, \tag{51}$$

the atoms are squeezed if either $(\Delta y)^2$ or $(\Delta p_y)^2$ is less than 1/2. The squeezing of atomic ensembles is usually defined in terms of the collective operators [46,47]. Because the angular momentum operators obey the commutation relation $[J_+,J_-]=2J_z$, the uncertainty relation $(\Delta J_x)^2(\Delta J_y)^2\geqslant\frac{1}{4}|\langle J_z\rangle|^2$ holds for any state. By substituting the Holstein-Primakoff forms into this expression and taking the thermodynamic limit, we see that this relation reduces to $(\Delta y)^2(\Delta p_y)^2\geqslant 1/4$, demonstrating the equivalence in the thermodynamic limit of our definition in terms of y and p_y and the usual one. In the normal phase, the expressions for the variances are evaluated by simply making the appropriate substitutions from Appendix A and taking their ground-state expectation value. In the super-radiant phase, it can be shown that the variances of the original field and atomic modes of Eqs. (50) and (51) can be expressed in terms of the displaced coordinates as follows:

$$(\Delta x)^2=(\Delta x')^2=(\Delta X)^2,\quad (\Delta p_x)^2=(\Delta p_x')^2=(\Delta P_X)^2,$$

$$(\Delta y)^2=(\Delta y')^2=\sqrt{\tilde{\omega}/\omega_0}(\Delta Y)^2\quad ,$$

$$(\Delta p_y)^2=(\Delta p_y')^2=\sqrt{\tilde{\omega}/\omega_0}(\Delta P_Y)^2. \tag{52}$$

This results from the fact that the squeezing variances do not depend upon the displacements of the field modes, and thus evaluating the super-radiant variances is as simple as in the normal phase.

The analytic values of these variances in the ground state are shown in Appendix B and are plotted as functions of coupling in Fig. 8. In the normal phase, as λ approaches λ_c there is a sharp increase, and eventually a divergence, in $(\Delta x)^2$ and $(\Delta y)^2$. This is accompanied by a slight squeezing

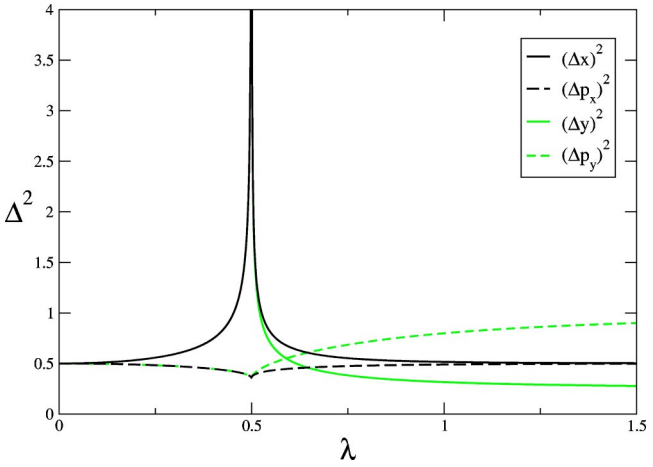

FIG. 8. The squeezing variances of the ground state of the DH in the thermodynamic limit. The Hamiltonian is on scaled resonance: $\omega=\omega_0=1$, $\lambda_c=0.5$. Note that on resonance, $(\Delta x)^2$ and $(\Delta y)^2$ are coincident for $\lambda<\lambda_c$, and the same for $(\Delta p_x)^2$ and $(\Delta p_y)^2$.

of the momentum variances. In the super-radiant phase, the initially divergent values of $(\Delta x)^2$ and $(\Delta y)^2$ reduce rapidly with increasing coupling. The behavior of these variances reflects the nature of the wave functions plotted in Figs. 5 and 6. Notice that as $\lambda\to\infty$, $(\Delta x)^2$ and $(\Delta p_x)^2$ return to their $\lambda=0$ values, whereas $(\Delta y)^2$ and $(\Delta p_y)^2$ become squeezed and antisqueezed, respectively. This is in agreement with the results of Eq. (48), which show that the e_1 mode becomes identical to the c mode, which is unsqueezed, whereas the e_2 mode reverts to a linear superposition of d and $d^\dagger$ operators, which is a specific example of the Bogoliubov transformation producing a squeezed state [48].

IV. THE ONSET OF CHAOS

As we have just demonstrated, the DH is exactly integrable in the thermodynamic limit. However, for finite j this is not the case, and the possibility of quantum chaos remains. The signature of quantum chaos which we use to investigate this possibility is the character of the energy spectrum as quantified by the nearest-neighbor level distribution $P(S)$. Bohigas *et al.* [5] first conjectured that the study of spectral quantities such as $P(S)$, and their comparison with the results from random matrix theory should give an indication of quantum chaos. This may be understood by the following argument. Classically integrable systems have high degrees of symmetry and hence their quantum counterparts have many conserved quantum numbers. This permits level crossings to occur in the spectrum, leading to a $P(S)$ with a maximum at small level spacing, $S\to 0$, with a $P(S)$ given by the Poissonian distribution $P_{\mathrm{P}}(S)=\exp(-S)$. We shall call quantum spectra with Poissonian statistics ''quasiintegrable.'' Conversely, classically chaotic systems have no such integrals of motion and we thus expect their quantum energy spectra to be highly correlated and absent of crossings, leading to $P(S)\to 0$ as $S\to 0$. Although the precise form of the $P(S)$ for chaotic systems depends on the symmetries of the

model, we shall find that only the Wigner-Dyson distribution, $P_W(S)=\pi S/2\exp(-\pi S^2/4)$, is of relevance here [49].

Despite its popularity, it should be pointed out that the correspondence between the $P(S)$ distribution and the integrability or otherwise of the classical system is not absolute, and exceptions do exist [50,51]. Despite this, the $P(S)$ does provide a convenient and useful indication of quantum chaos, and the conjecture does hold true in countless examples. In the present case, this signature turns out to be very accurate, as will be evinced when we compare the $P(S)$ results with those of our semiclassical model.

A. Numerical diagonalization

Exact solutions for the DH at finite j do not exist, except in the very special case of $j=1/2$, where isolated exact ("Juddian") solutions may be found [52,53]. Consequently, we employ numerical diagonalization to investigate the system. To perform these diagonalizations we use the basis $\{|n\rangle\otimes|j,m\rangle\}$, where $|n\rangle$ are number states of the field and $|j,m\rangle$ are the Dicke states. In performing the diagonalization, we truncate the bosonic Hilbert space, but always maintain the full Hilbert space of the pseudospin. The size of the matrices requiring diagonalization is reduced by restricting ourselves to a single-parity subspace, which is achieved by only considering states with $n+m+j$ even or odd for positive and negative parity, respectively. With j finite, Π is a good quantum number, independent of coupling, and the ground state always has positive parity.

The results obtained via this diagonalization for the ground-state energy and its second derivative for a sequence of finite j values are plotted alongside the $j\to\infty$ results in Fig. 3, while the corresponding atomic inversions and mean photon numbers are plotted in Fig. 4. These figures demonstrate how rapidly the finite j results approach their thermodynamic limits as j is increased.

B. Level statistics

Having numerically obtained the energy spectra of the DH, we can construct the nearest-neighbor level-spacing distribution $P(S)$. This is formed from a large number of levels from the spectrum, which we initially unfold to remove secular variation [49]. We then calculate the level spacings

$$S_n=E_{n+1}-E_n, \tag{53}$$

where $\{E_n;\ n=0,1,\ldots\}$ is the set of eigenenergies of the DH with positive parity, and construct their distribution function $P(S)$. Finally, we normalize the results for comparison with the universal ensembles of random matrix theory [49].

Figure 9 shows the $P(S)$ distributions obtained for the DH at various values of λ and j. At low j ($j\leqslant 3$), the $P(S)$ clearly do not correspond to any of the universal ensembles, but rather to nongeneric distributions consisting of several isolated peaks. This is most obvious in the $j=1/2$ case (not shown here), which is known as the Rabi Hamiltonian (RH) [54]. The RH has a spectrum that is of "picket-fence" character [35], which is characteristic of genuinely integrable models such as one-dimensional systems and systems of harmonic oscillators [4]. The RH is unusual and must be treated as a special case because, although it has never been shown to be integrable, isolated exact solutions do exist [52,53]. Moreover, the model is separable and may be reduced to a single degree of freedom [32].

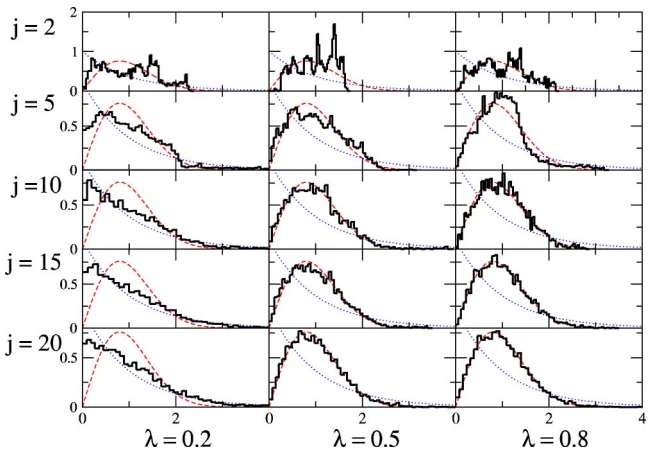

FIG. 9. Plots of nearest-neighbor distributions $P(S)$ for the Dicke Hamiltonian for different couplings λ and pseudospin j. Also plotted are the universal Poissonian (dots) to Wigner (dashes) distributions. The Hamiltonian is on scaled resonance: $\omega=\omega_0=1$, $\lambda_c=0.5$.

Returning to the $P(S)$ distributions, we see that at low couplings $\lambda<\lambda_c$ [for example, $\lambda=0.2$ in Fig. (9)], as we increase j, the $P(S)$ loses its nongeneric features and approaches even closer the Poissonian distribution $P_P(S)$. At and above the critical coupling ($\lambda=0.5$ and 0.8 in Fig. 9), the spectrum is seen to converge onto the Wigner-Dyson distribution $P_W(S)$ as j is increased.

The nature of the change in the $P(S)$ distribution may be characterized by the quantity

$$\eta\equiv\left|\frac{\int_0^{S_0}[P(S)-P_W(S)]dS}{\int_0^{S_0}[P_P(S)-P_W(S)]dS}\right|, \tag{54}$$

where $S_0=0.472\,913\ldots$, the value of S at which the two generic distributions $P_P(S)$ and $P_W(S)$ first intersect [10]. η measures the degree of similarity of the calculated $P(S)$ to the Wigner surmise $P_W(S)$, and is normalized such that if $P(S)=P_W(S)$ then $\eta=0$, and if $P(S)=P_P(S)$ then $\eta=1$. The behavior of η as a function of coupling for $j=5$ and $j=20$ is shown in Fig. 10. Considering the $j=20$ case first, we see that the spectrum is strongly Poissonian at low couplings, and that as λ is increased towards λ_c it becomes more Wigner-Dyson–like. This proceeds until we reach λ_c, about which the spectrum is remarkably well described by $P_W(S)$. Note that for $\lambda<\lambda_c$ the value of η drops steadily with coupling, whereas above λ_c it maintains an approximately constant value close to zero. For the $j=5$ case, a similar transition is observed, but it is not as pronounced and the agreement with the universal distributions is not as good as in the higher j case.

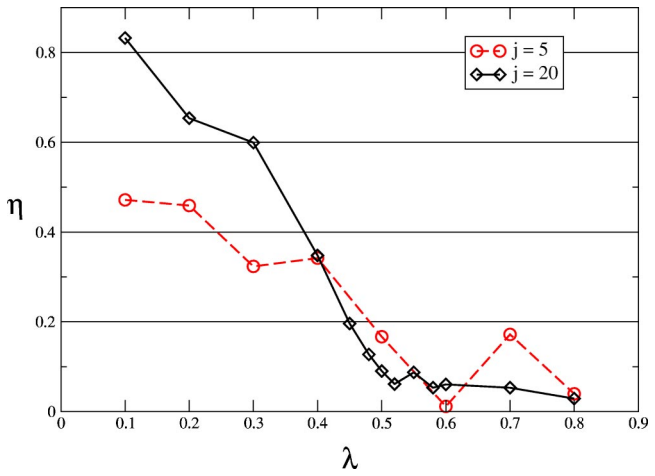

FIG. 10. The modulus of η, Eq. (54), plotted as a function of coupling for systems of $j=5$ and $j=20$. A value of $\eta=1$ indicates Poissonian statistics and $\eta=0$ corresponds to the Wigner-Dyson distribution. The system is on scaled resonance ($\omega=\omega_0=1$).

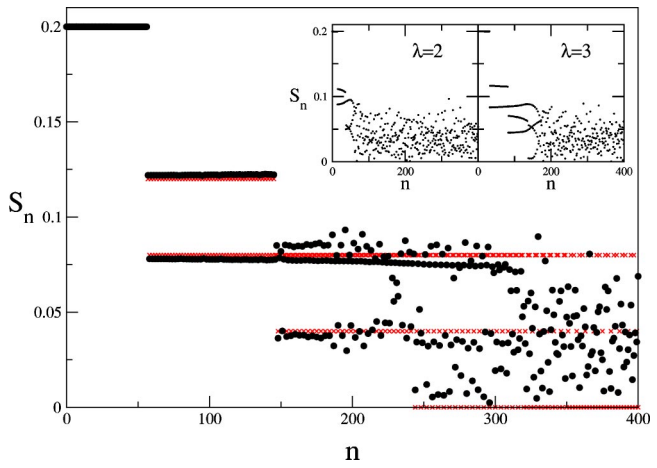

FIG. 11. Nearest-neighbor spacing $S_n=E_{n+1}-E_n$ vs eigenvalue number n plot for $j=5$ with $\lambda=4$. Horizontal crosses: results for the integrable $\lambda\to\infty$ Hamiltonian. Inset: $j=5$ results with $\lambda=2$ and $\lambda=3$. The Hamiltonian is on scaled resonance: $\omega=\omega_0=1$, $\lambda_c=0.5$.

Thus, for sufficiently high j, we see a significant change in $P(S)$ as λ is increased from zero through the critical value λ_c. Below λ_c, there is a significant amount of level crossing, which decreases as we approach λ_c. Above λ_c, there is practically none, to within statistical error. Thus, we conclude that the precursors of the QPT in this model lead to a crossover from quasiintegrable to quantum-chaotic behavior at $\lambda\approx\lambda_c$ for sufficiently high j.

C. Regularity at low energy

A further transition between integrable and chaotic behavior is observed in the sequence of level spacings S_n as the coupling is increased from λ_c to ∞. In the $\lambda\to\infty$ limit, the DH is integrable for arbitrary j and equivalent to

$$H_{\lambda\to\infty}=\omega a^\dagger a+2\frac{\lambda}{\sqrt{2j}}(a^\dagger+a)J_x. \tag{55}$$

The eigenstates of $H_{\lambda\to\infty}$ are obviously eigenstates of J_x, and thus

$$H_{\lambda\to\infty}=\omega a^\dagger a+2m\frac{\lambda}{\sqrt{2j}}(a^\dagger+a), \tag{56}$$

where $m=-j,\ldots,j$ is the eigenvalue of J_x. This bosonic Hamiltonian is diagonalized by the displacement $a\to a-2m\lambda/\sqrt{2j}$, giving the eigenvalues to be

$$E_{km}=\frac{\omega}{j}k-\frac{2\lambda^2}{\omega j^2}m^2, \tag{57}$$

where $k=0,1,2,\ldots$. The energy levels with $+m$ and $-m$ are degenerate.

As λ is increased from λ_c to approach this $\lambda\to\infty$ limit with j fixed, the spectrum reverts from Wigner-like to integrable. However, it does not follow the usual transition sequence of the Wigner distribution, gradually changing into a Poissonian one, as one might expect, but rather through a sequence illustrated in Fig. 11. For couplings sufficiently higher than λ_c, the spectrum becomes very regular at low energy, where it approximates the $\lambda\to\infty$ results very closely. Outside the regular region the spectrum is well described by the Wigner surmise, and the energy scale over which the change between the two regimes occurs is seen to be surprisingly narrow. As coupling is increased, the size of the low-energy integrable window increases, until it eventually engulfs the whole spectrum as $\lambda\to\infty$. This division of the spectrum into regions is close to Percival's conception of how regular and irregular behavior would manifest itself in quantum systems [55].

D. Wave functions for finite j

We now consider the wave functions of the DH at finite j. To do this, we shall use the position-momentum representation of Eq. (13) used earlier in discussing the wave functions in the thermodynamic limit. We begin with the eigenfunctions obtained from numerical diagonalization, which are of the form

$$|\Psi_{nm}\rangle=\sum_{n=0}^{n_c}\sum_{m=-j}^{+j}c_{nm}^{(j)}|n\rangle|j,m\rangle, \tag{58}$$

where n_c is the maximum boson number in the artificially truncated Fock space, and $c_{nm}^{(j)}$ are coefficients. The position representatives of the number states of the field $|n\rangle$ are simply the usual harmonic oscillator eigenfunctions

$$\langle x|n\rangle=\frac{1}{2^n n!}\sqrt{\frac{\omega}{\pi}}e^{-(1/2)\omega x^2}H_n(\sqrt{\omega}x), \tag{59}$$

where H_n is the nth Hermite polynomial. For the angular momentum part of the basis vector, we recall that under the Holstein-Primakoff mapping, $J_z\to b^\dagger b-j$ and, thus, the

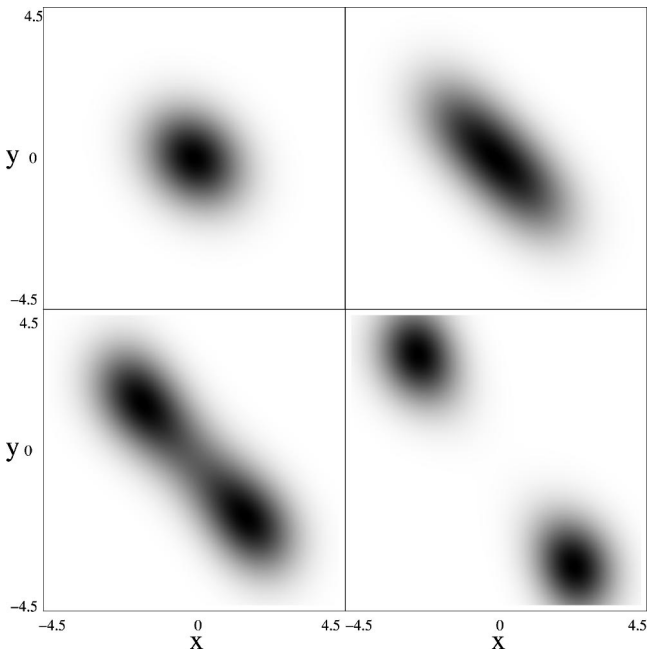

FIG. 12. The modulus of the ground-state wave function $\psi(x,y)$ of the Dicke Hamiltonian in the abstract x-y representation for finite $j=5$, at couplings of $\lambda/\lambda_c=0.4$, 1.0, 1.2, 1.4. Black corresponds to $\max|\psi|$ and white corresponds to zero. The Hamiltonian is on scaled resonance $\omega=\omega_0=1$, $\lambda_c=0.5$.

Dicke states are eigenstates of $b^\dagger b$ with eigenvalue $(j+m)$: $b^\dagger b|j,m\rangle=(j+m)|j,m\rangle$, $-j\leqslant m\leqslant j$. Consequently, we may represent the Dicke states in the same way as the Fock states above, allowing us to write the total wave function in the two-dimensional position representation as

$$\Psi_{nm}(x,y)=\frac{\sqrt{\omega\omega_0}}{\pi}e^{-1/2(\omega x^2+\omega_0 y^2)}\sum_{n=0}^{n_c}\sum_{m=-j}^{+j}c_{nm}^{(j)} \times\frac{H_n(\sqrt{\omega}x)H_{j+m}(\sqrt{\omega_0}y)}{2^{(n+j+m)}\,n!(j+m)!}. \tag{60}$$

This is a very productive representation in which to study this Hamiltonian. It does, however, suffer from the drawback that whereas the set of oscillator eigenfunctions Eq. (59) forms an orthonormal set in the x direction, this is not the case in the y direction as we only keep up to the $(2j)$th oscillator eigenfunction in this direction. This means, for example, that we could not go from an arbitrary wave function in the y direction to a description in terms of the Dicke states because we do not have a complete set of functions in this direction. Specifically, the significant width of the wave function is limited in the y direction by the maximum significant extent of the highest Hermite polynomial H_{2j}. However, if we know the value of j and only consider wave functions that are describable in terms of these, then the representation is unique.

Figure 12 shows the ground-state wave function of the DH with $j=5$ for a series of increasing couplings. Note that the wave function is always invariant under a rotation of π about the origin as demanded by the Π symmetry. This wave function starts as a single lobe centered at the origin for low coupling. As the coupling increases, the two modes start mixing, leading to a stretching of the single-peaked wave function, which then splits into two as coupling is increased through a coupling approximately equal to λ_c. On further increasing the coupling, the two lobes move away from each other in their respective quadrants of the x-y plane.

The key observation regarding the two lobes formed above λ_c is that, provided j and λ are both sufficiently large, their displacement from each other is proportional to $\sqrt{j}$, and that this is a macroscopic quantity. The excited states exhibit a similar behavior, having an extent proportional to $\sqrt{j}$ above the phase transition.

Therefore, around the critical coupling $\lambda\approx\lambda_c$, the wave functions of the system become delocalized, and the extent of this delocalization is proportional to $\sqrt{j}$. As this is a macroscopic quantity, we see that above λ_c, the system at finite j develops macroscopic coherence in its wave functions. The most striking example of this is the ground state, where the two macroscopically different lobes are reminiscent of the two states of a Schrödinger cat.

The delocalization and the accompanying macroscopic coherence are rather general features of the onset of chaos, and are natural consequences of the exponential divergence of trajectories in a classically chaotic system [56]. If we consider a small volume of initial conditions in the classical phase space (a well-localized initial wave packet), and let the system evolve chaotically, this initial volume rapidly becomes blurred out over the entire phase space accessible to it. This is reflected in the quantum system by the delocalization of the wave functions. That such systems are macroscopically coherent may be seen from the observation that under Hamiltonian dynamics, the volume of the initial ''wave packet'' remains constant in time (Liouville's theorem). This means that the exponential divergence in some direction leads to the exponential contraction in others. This contraction will continue until the size of the packet becomes of the order of $\hbar$ and quantum effects come into play. If we imagine that the wave packet becomes narrow in the direction of momentum p, then the uncertainty Δp becomes very small. In order that the Heisenberg uncertainty relation holds, the uncertainty in the corresponding coordinate Δx must become very large, and this leads to the emergence of macroscopic coherence in the system.

This effect is what was observed in the variances calculated earlier in connection with squeezing in the thermodynamic limit. As $\lambda\rightarrow\lambda_c$ from below, the variances $(\Delta x)^2$ and $(\Delta y)^2$ diverged, with $(\Delta p_x)^2$ and $(\Delta p_y)^2$ remaining near their quantum limit of 1/2. The behavior of these variances then reflects the onset of quantum chaos and the macroscopic coherence of the wave functions. A vital difference between the $j\rightarrow\infty$ and the finite j results thus emerges in the superradiant phase. In the thermodynamic limit, the variances $(\Delta x)^2$ and $(\Delta y)^2$ reduce as λ is increased from λ_c, indicating that the wave functions become localized and lose this macroscopic coherence. This is in contrast with the finite j, where sufficiently above λ_c the wave function is always delocalized and the variances are $O(\sqrt{j})$. This is because,

whereas at finite j we obey Π symmetry and thus have both the lobes of the wave function, in the thermodynamic limit we consider each lobe separately under the broken symmetry. The individual lobes are themselves localized and this is where the discrepancy arises. This is, we believe, the reason why, although the spectrum is of the Wigner-Dyson type for large j, the spectrum in the $j\to\infty$ limit is integrable, since in this limit the wave functions possess no delocalization and no macroscopic coherence.

This picture also provides us with an explanation of why $P(S)$ for very small j are of the nongeneric one-dimensional type. As the extent of the wave function in the y direction is effectively constrained by the number of harmonic eigenfunctions in that direction, which is determined by j, having a small j prevents full delocalization in this direction, inhibiting the chaoticity of the quantum system.

V. THE SEMICLASSICAL MODEL

As noted in the Introduction, there have been many different semiclassical models derived from the DH [36–39]. That there have been so many different approaches is a reflection of the fact that the quantum-mechanical spin possesses no direct classical analog. Nevertheless, semiclassical models can be constructed, and in the following we shall propose a different approach. Before this, let us briefly examine some of the previous work.

A widely discussed approach is that of a Hartree-Fock–type approximation in which one derives the Heisenberg equations of motion for the system and replaces the operators in these equations by their expectation values [32]. These are treated as classical variables and a set of nonlinear equations of motion are obtained for them, which show classical chaos for certain parameter ranges [37]. Despite this, the above approach is not completely satisfactory as the motion only depends on j in a trivial way. Furuya *et al.* have studied a classical model similar to the one we propose below [36]. They derived their semiclassical Hamiltonian by evaluating the expectation value of the DH in a state composed of a product of photonic and atomic coherent states, and this system was also shown to exhibit chaos. Despite the similarity of their model to ours, they did not discuss the role of the phase transition in determining the chaoticity of the model, which is a key feature of our model.

We start with the DH in the bosonic form of Eq. (10):

$$H=\omega_0(b^\dagger b-j)+\omega a^\dagger a + \lambda(a^\dagger+a)\left(b^\dagger\sqrt{1-\frac{b^\dagger b}{2j}}+\sqrt{1-\frac{b^\dagger b}{2j}}b\right). \quad (61)$$

By using the inverse of the relations in Eq. (13), namely

$$a\equiv\sqrt{\frac{\omega}{2}}\left(x+\frac{i}{\omega_0}p_x\right),\quad a^\dagger\equiv\sqrt{\frac{\omega}{2}}\left(x-\frac{i}{\omega_0}p_x\right),$$
$$b\equiv\sqrt{\frac{\omega_0}{2}}\left(y+\frac{i}{\omega_0}p_y\right),\quad b^\dagger\equiv\sqrt{\frac{\omega_0}{2}}\left(y-\frac{i}{\omega_0}p_y\right), \quad (62)$$

we may write this Hamiltonian in the position-momentum representation,

$$H=-j\omega_0+\frac{1}{2}(\omega^2x^2+p_x^2-\omega+\omega_0^2y^2+p_y^2-\omega_0) + \lambda\sqrt{\omega\omega_0}x\left\{\left(y-\frac{i}{\omega_0}p_y\right)\sqrt{1-\eta}+\sqrt{1-\eta}\left(y+\frac{i}{\omega_0}p_y\right)\right\}, \quad (63)$$

where we have written

$$\eta=(\omega_0^2y^2+p_y^2-\omega_0)/(4j\omega_0). \quad (64)$$

We now move very naturally from this quantum-mechanical Hamiltonian to a semiclassical one by setting the position-momentum commutators to zero, i.e., $[x,p_x]=0$, and $[y,p_y]=0$. This causes the interaction term to become real, and in terms of classical variables we have

$$H_{\rm sc}=-j\omega_0+\frac{1}{2}(\omega^2x^2+p_x^2-\omega+\omega_0^2y^2+p_y^2-\omega_0) + 2\lambda\sqrt{\omega\omega_0}xy\sqrt{1-\frac{\omega_0^2y^2+p_y^2-\omega_0}{4j\omega_0}}. \quad (65)$$

Unusually, this Hamiltonian contains an intrinsic constraint that is determined by the requirement that the square root must remain real for the system to remain Hamiltonian. This means that the inequality

$$\eta=\frac{1}{4j\omega_0}(\omega_0^2y^2+p_y^2-\omega_0)\leqslant 1 \quad (66)$$

is satisfied for all times.

A. Classical phase transition

The Hamiltonian $H_{\rm sc}$ undergoes a spontaneous symmetry-breaking phase transition that is directly analogous to the QPT of the quantum model. The exact correspondence between the classical and quantum Hamiltonians in the thermodynamic limit is because in this limit the system is exactly described with a mean-field theory as used earlier, and the use of classical variables as we have done here is equivalent to a mean-field theory. Consequently, we are able to derive classical effective Hamiltonians exactly as we did in the quantum case. The effective Hamiltonian for the normal phase is derived by simply letting $j\to\infty$ (i.e., $\eta\to 0$) in the Hamiltonian of Eq. (65). This gives us

$$H_{\rm sc}^{(1)}=\frac{1}{2}\{\omega^2x^2+p_x^2+\omega_0^2y^2+p_y^2+4\lambda\sqrt{\omega\omega_0}\ xy-\omega_0-\omega\} - j\omega_0, \quad (67)$$

which is identical to Eq. (14) from the quantum analysis, and may be diagonalized with the same rotation. The equilibrium position of Hamiltonian $H_{\rm sc}^{(1)}$ is the origin: $x=y=p_x=p_y=0$.

An effective Hamiltonian for the super-radiant phase is derived in the same way as in the quantum case, by displacing the coordinates as in Eq. (45), so that $x\rightarrow x'\pm\Delta_x, y\rightarrow y'\mp\Delta_y$, where the displacements are the same as before: $\Delta_x\equiv\sqrt{2\alpha/\omega}$ and $\Delta_y\equiv\sqrt{2\beta/\omega_0}$. Making these displacements and then taking the thermodynamic limit results in a Hamiltonian $H_{\rm sc}^{(2)}$ that is identical with the quantum Hamiltonian $H^{(2)}$ of Eq. (29) in the appropriate position-momentum representation, which may thus be diagonalized with the same rotation. The equilibrium positions of $H_{\rm sc}^{(2)}$ are $(+\Delta_x, -\Delta_y)$ and $(-\Delta_x,+\Delta_y)$.

The bounds on the existence of these classical effective Hamiltonians are exactly as in the quantum case—the excitation energies $\varepsilon_{-}^{(1)}$ and $\varepsilon_{-}^{(2)}$ of the decoupled modes remain real only on their respective sides of the critical coupling λ_c, which has the same value as in the quantum case. Clearly, the semiclassical system is completely integrable in this thermodynamic limit.

B. Equations of motion

To analyze the behavior of this semiclassical system for finite j, we form Hamilton's equations of motion from the derivatives of $H_{\rm sc}$ [57]

$$\dot{x}=p_x,$$

$$\dot{y}=p_y\left(1-\frac{\lambda}{2j}\sqrt{\frac{\omega}{\omega_0}}\frac{xy}{\sqrt{1-\eta}}\right),$$

$$\dot{p}_x=-\omega^2x-2\lambda\sqrt{\omega\omega_0}\ y\sqrt{1-\eta},$$

$$\dot{p}_y=-\omega_0^2y-2\lambda\sqrt{\omega\omega_0}x\sqrt{1-\eta}\left(1-\frac{\omega_0y^2}{4j(1-\eta)}\right), \quad (68)$$

where as before

$$\eta=\frac{1}{4j\omega_0}(\omega_0^2y^2+p_y^2-\omega_0). \quad (69)$$

It is not *a priori* obvious that this flow should preserve the condition set out in Eq. (66). However, we have demonstrated numerically that, provided we choose initial conditions that satisfy Eq. (66), then this condition is always satisfied. Although we have not shown this analytically, it can at least be seen to be plausible. Calculating $\dot{\eta}=d\eta/dt=\{H,\eta\}$, where $\{\cdots\}$ denote Poisson brackets, we find that

$$\dot{\eta}=-\frac{\lambda}{j}\sqrt{\frac{\omega}{\omega_0}}xp_y\sqrt{1-\eta}, \quad (70)$$

so that as η approaches unity its rate of change approaches zero, implying that it is bound appropriately.

We now determine the fixed points of this flow at finite j by setting $\dot{x}=\dot{y}=0$, $\dot{p}_x=\dot{p}_y=0$. The simplest fixed point is given by $x=y=p_x=p_y=0$, the coordinate origin. By calculating the Hessian stability matrix from the second derivatives of H, we see that this fixed point is only stable when

$$\frac{1}{2}\{\omega^2+\omega_0^2-\sqrt{(\omega^2-\omega_0^2)+16\lambda^2\omega\omega_0(1+1/(4j))}\}>0, \quad (71)$$

i.e., when

$$\lambda<\frac{\lambda_c}{\sqrt{1+1/(4j)}}. \quad (72)$$

There are two other fixed points, both of which have $p_x=p_y=0$, and with x and y given by

$$x_0=\pm\frac{2\lambda}{\omega}\sqrt{\frac{j}{\omega}\left\{\left(1+\frac{1}{4j}\right)^2-\frac{\lambda_c^4}{\lambda^4}\right\}},$$

$$y_0=\mp\sqrt{\frac{2j}{\omega}\left(1+\frac{1}{4j}-\frac{\lambda_c^2}{\lambda^2}\right)}. \quad (73)$$

These two quantities only remain real, provided that $1+(1/4j)-(\lambda_c^2/\lambda^2)>0$, which corresponds to the condition

$$\lambda>\frac{\lambda_c}{\sqrt{1+1/(4j)}}. \quad (74)$$

Provided that the above condition is fulfilled, the fixed points given by $(+x_0,-y_0)$ and $(-x_0,+y_0)$ exist and are stable. So, below the coupling $\lambda_c/\sqrt{1+1/(4j)}$, only one fixed point exists, which lies at the coordinate origin and is stable. Above $\lambda=\lambda_c/\sqrt{1+1/(4j)}$, this fixed point becomes unstable and two new stable fixed points appear at the coordinates $(+x_0,-y_0)$ and $(-x_0,+y_0)$. Note that these expressions give us the first correction to the location of the critical coupling in terms of a perturbation series in j. We can consider this semiclassical system as a particle moving in the two-dimensional, momentum-dependent potential

$$U(x,y,p_y)=\frac{1}{2}(\omega^2x^2+\omega_0^2y^2)+2\lambda\sqrt{\omega\omega_0}xy\sqrt{1-\frac{+p_y^2-\omega_0}{4j\omega_0}}. \quad (75)$$

Maps of this potential for different values of increasing coupling and for two different values of p_y are shown in Fig. 13. First, note how significantly the value of p_y affects the shape of the potential felt by the ''particle.'' For example, above λ_c at $\lambda=0.8$, with $p_y=0$, the potential bifurcates into two separate wells, whereas for $p_y=3$ it does not. Also note the similarity between the plot of $U(x,y,p_y)$ for $p_y=0$ and the plot of the wave function in Fig. 12. It is clear that the $p_y=0$ potential largely determines the structure of the wave func-

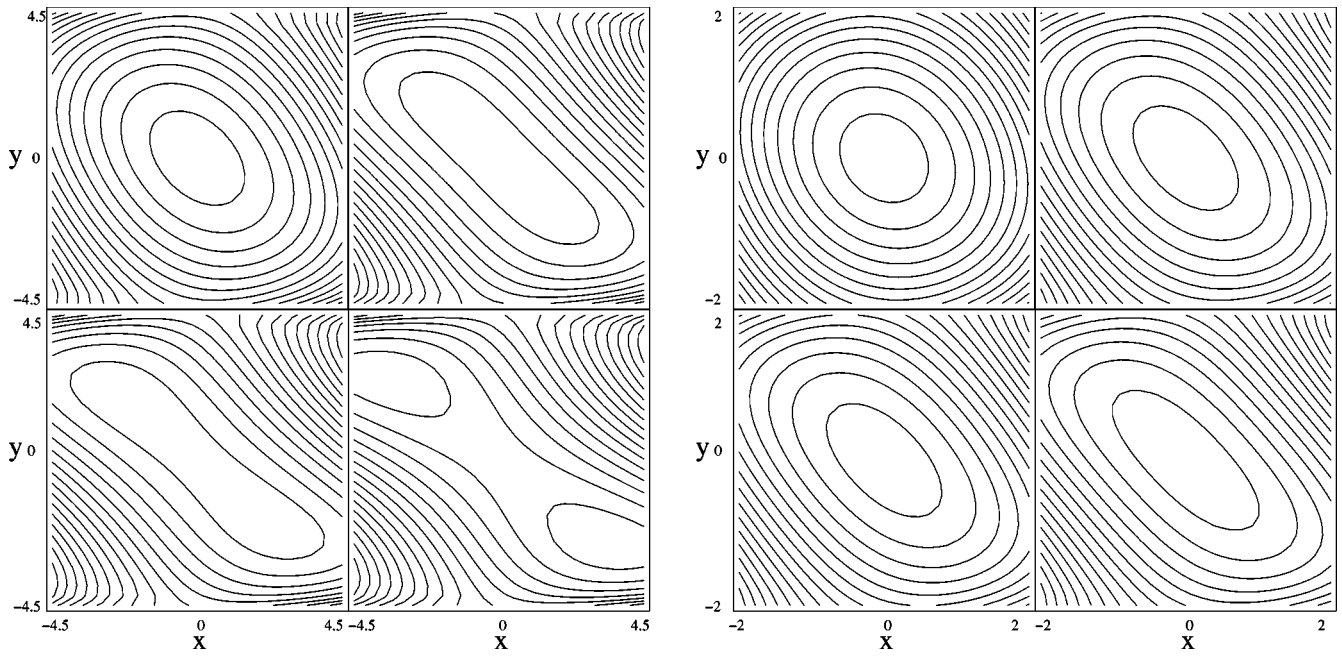

FIG. 13. The momentum-dependent potential $U(x,y,p_y)$ at two different values of momentum $p_y=0$ (left) and $p_y=3$ (right) for a series of couplings the same as in Fig. (12). Note the difference in scales between the two plots. The Hamiltonian is on scaled resonance: $\omega=\omega_0=1$, $\lambda_c=0.5$.

tion at finite j, presumably because the location of the fixed points are determined with $p_y=0$.

C. Chaos in the semiclassical model

We numerically integrate Hamilton's equations of motion for the semiclassical system for a variety of different parameters and initial conditions. In order to analyze the trajectories resulting from these integrations, we use Poincaré sections through the four-dimensional phase space. As this system is Hamiltonian, the energy

$$E=-j\omega_0+\frac{1}{2}(\omega^2x^2+p_x^2-\omega+\omega_0^2y^2+p_y^2-\omega_0)+2\lambda\sqrt{\omega\omega_0}\,xy\sqrt{1-\eta} \tag{76}$$

is conserved, and thus we define our surface of section by $p_x=0$ with, p_y being fixed by the energy E. We only record traversals for $p_y>0$. Poincaré sections for illustrative parameter values are shown in Fig. 14.

At low λ ($\lambda\leqslant 0.4$ in Fig. 14), the Poincaré sections consist of a series of regular, periodic orbits. Approaching the critical coupling ($\lambda=0.44$,0.5 in Fig. 14), we see a change in the character of the periodic orbits, and also the emergence of a number of chaotic trajectories. Increasing the coupling further results in the breakup of the remaining periodic orbits and the whole phase space becomes chaotic for couplings a little over the critical value ($\lambda=0.6$ in Fig. 14). This transition to chaos in the classical system mirrors very closely that seen in the quantum system, especially in the way that most of the change in the nature of the behavior is centered about the critical coupling determined by the phase transition. An interesting feature of this classical Hamiltonian is that the (re)quantization of this Hamiltonian is not unique. This is because the potential $U(x,y,p_y)$ depends on the momentum p_y, a situation that may be compared to the quantization of a Lagrangian for an electron in a magnetic field, where an extra ''rule'' is required to obtain the correct quantization. We may requantize $H_{\rm sc}$ by simply reversing the steps in Eqs (61)–(65). However this is not the most obvious path, since it involves the addition of extra, imaginary, p_y-dependent terms that have canceled in the final Hamiltonian. Alternatively, one may simply requantize Eq. (65) as it stands, which results in the Hamiltonian

$$H'=\omega_0(b^\dagger b-j)+\omega a^\dagger a+\lambda(a^\dagger+a)(b^\dagger+b)\sqrt{1-\frac{b^\dagger b}{2j}}, \tag{77}$$

which is clearly different to the original bosonic Hamiltonian of Eq. (61). This ambiguity disappears in the thermodynamic limit, since here $U(x,y,p_y)$ becomes momentum independent in this limit in both systems phases.

We note that the classical Hamiltonian

$$H''=-j\omega_0+\frac{1}{2}(\omega^2x^2+p_x^2-\omega+\omega_0^2y^2+p_y^2-\omega_0)+2\lambda\sqrt{\omega\omega_0}xy\sqrt{1-\frac{\omega_0^2y^2-\omega_0}{4j\omega_0}}, \tag{78}$$

which is the same as the original Hamiltonian of Eq. (65), but with p_y^2 removed from the square root it displays a similar behavior to that of the full Hamiltonian. The gain in simplicity in using this model suggests that it would be an ideal test model for further exploration of the dynamics of this

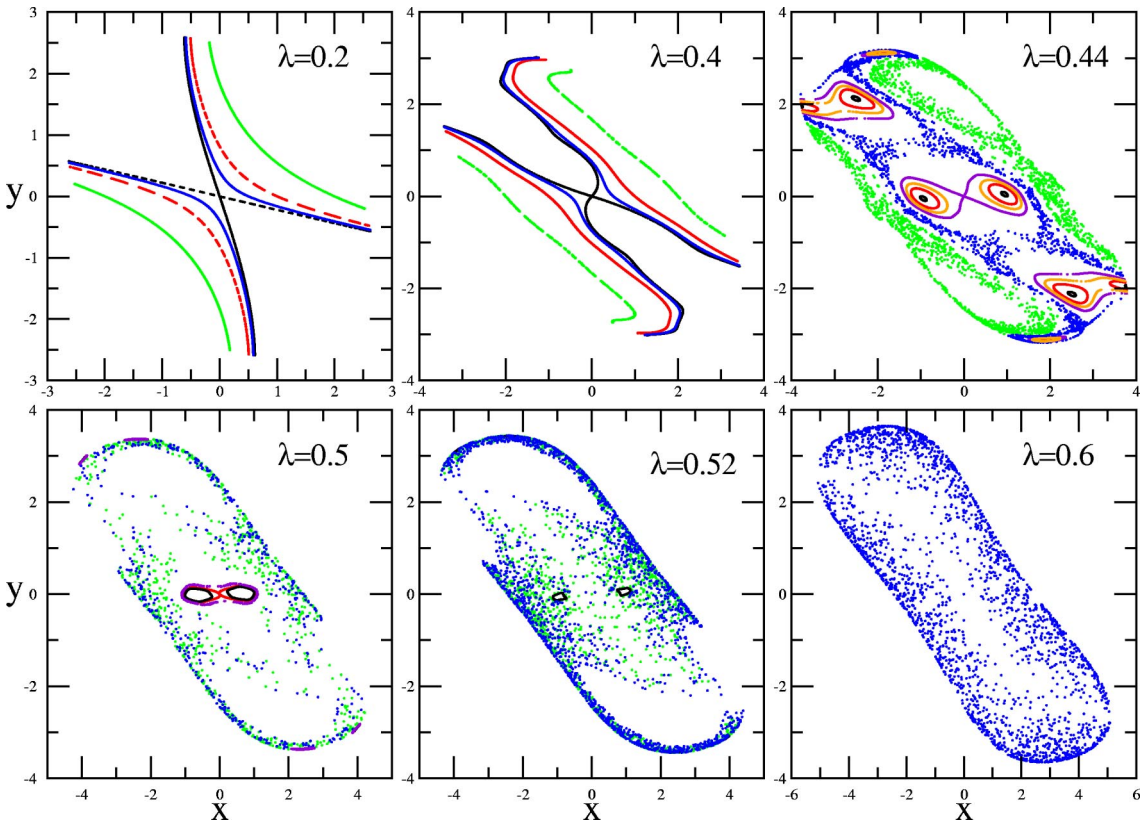

FIG. 14. Poincaré sections for the classical Dicke model for a sequence of increasing couplings, with $j=5$ and $E=-3$. The Hamiltonian is on scaled resonance $\omega=\omega_0=1$; $\lambda_c=0.5$.

type of Hamiltonian constrained by a square-root. The behavior of the Hamiltonian H'', and the fact that the $p_y=0$ potential largely dominates the dynamics of H_{cl} and the structure of the wave function of the original DH suggest that the requantization route is not critical, provided that j is not small.

VI. THE RWA AND INTEGRABILITY

The DH in the RWA is given by

$$H_{\mathrm{RWA}}=\omega_0 J_z+\omega a^\dagger a+\frac{\lambda}{\sqrt{2j}}(a^\dagger J_-+aJ_+). \tag{79}$$

It is in this form that the DH is generally studied and in which the thermodynamics of the phase transition were originally discussed [25,26]. In the RWA, the QPT occurs at a coupling that is twice that of the non-RWA critical value $\lambda_c^{\mathrm{RWA}}=2\lambda_c=\sqrt{\omega\omega_0}$ [27,28]. This is simply a consequence of the fact that in the non-RWA DH there are four terms in the interaction, whereas here we only have two. As each term contributes to the mean field, the critical coupling of the RWA is twice as large as the non-RWA one.

In the RWA, the excitation number $\hat{N}$ of Eq. (8) becomes exactly conserved. This splits the total Hilbert space into an infinite number of subspaces, labeled by the excitation number $\hat{n}=0,1,2,\ldots$, which in turn leads to level crossings and to a Poisson distribution for $P(S)$. The crossover between the RWA and non-RWA $P(S)$ distributions has been studied by treating the non-RWA terms as a perturbation [34], and it was found that as the strength of this perturbation is increased from zero to one, a standard crossover between Poissonian and Wigner-Dyson statistics is observed.

Here, we report two observations concerning the difference between the RWA and non-RWA models. First, a calculational issue that arises when considering the RWA system in the thermodynamic limit. We may derive effective Hamiltonians in each phase by using the Holstein-Primakoff representation as before. In the normal phase, we obtain

$$H^{(1)}_{\mathrm{RWA}}=\omega_0 b^\dagger b+\omega a^\dagger a+\lambda(a^\dagger b+b^\dagger a)-j\omega_0. \tag{80}$$

The Bogoliubov transformations required to diagonalize this Hamiltonian are much simpler in terms of annihilation and creation operators than those for the non-RWA case. Specifically, the RWA diagonalizing transformations are

$$a\rightarrow -c_1\sin\beta+c_2\cos\beta;\quad b\rightarrow c_1\cos\beta+c_2\sin\beta, \tag{81}$$

plus the Hermitian conjugate relations, where the rotation angle β is given by

$$\tan(2\beta)=\frac{2\lambda}{\omega-\omega_0}. \tag{82}$$

The transformation for annihilation operators only involves annihilation operators, and the same with the creation

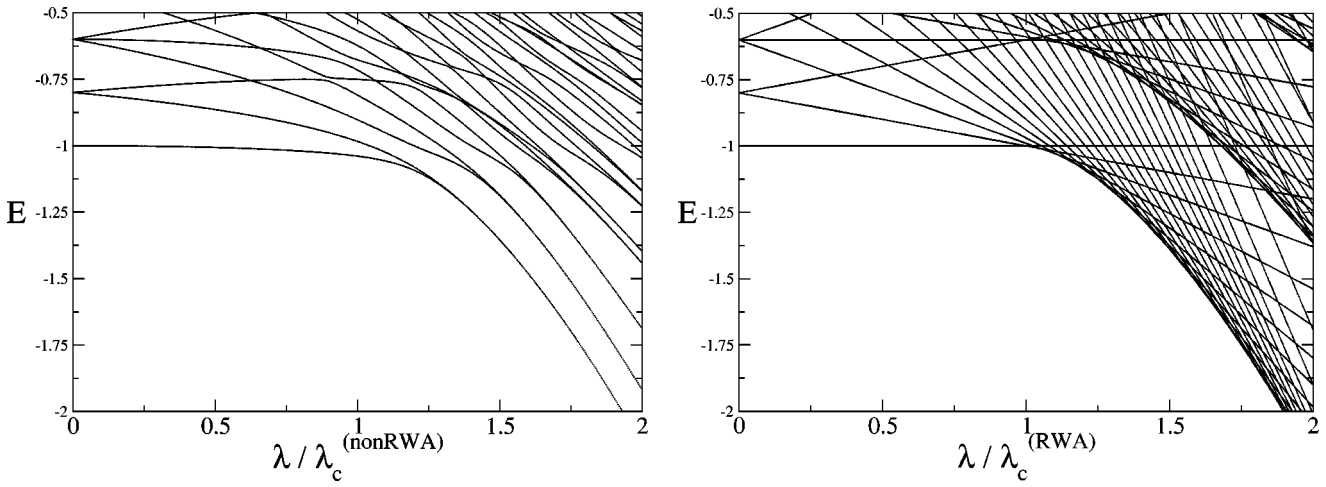

FIG. 15. The full energy schema of the (a) non-RWA and (b) RWA Dicke Hamiltonian for $j=5$. The Hamiltonian is on scaled resonance; $\omega=\omega_0=1$.

operators. This is in contrast with the non-RWA transformations, which transform any given operator into a linear combination of all four operators. Therefore, in the RWA it is very simple to find the diagonalizing transformation in the second quantized representation, whereas in the non-RWA case, this diagonalization only becomes transparent when one considers the first quantized position-momentum representation of the operators. The converse of this statement is true; it is hard to find the diagonalizing transformation in the RWA if one works in the position-momentum representation. We conjecture that this is a more general point than just applying here, and hope that this observation may be useful in other problems.

Our second observation concerns the comparison of the energy spectra at finite j of the RWA [58] and non-RWA Hamiltonians. Figure 15 shows two typical spectra, with coupling axes chosen for easy comparison. In terms of the appropriate critical coupling, the ground-state energy of the non-RWA spectrum is remarkably well approximated by the caustic of all the energy levels in the RWA spectrum that have negative slopes. As j increases, this approximation becomes better as the length of the individual line segments become shorter, until, in the thermodynamic limit, the correspondence of the ground states becomes exact and both excitation spectra become quasicontinuous.

VII. DISCUSSION

We have presented a coherent and comprehensive picture of how the existence of a QPT in the thermodynamic limit plays a crucial role in determining chaotic properties in a model interacting system. The DH exhibits a changeover from quasiintegrability to chaos, and this transition is located by the precursors of the QPT around the critical point, λ_c. This statement applies equally well to the original quantum system and to the semiclassical counterpart derived from it.

Our analysis of the DH in the thermodynamic limit consists of deriving an effective Hamiltonian to describe the system in each of its normal and super-radiant phases. For arbitrary coupling, the system is described in terms of two decoupled modes, each of which is a collective photon-atom excitation, and it is the vanishing of the excitation energy associated with the photonlike mode, that delimits the two phases. Our approach is particularly useful because we can calculate exactly any property of the system in the thermodynamic limit by simply utilizing the appropriate Bogoliubov transformations.

This analysis reveals that the QPT breaks the symmetry associated with the parity operator Π. In the normal phase, where the system in effectively unexcited, the wave functions of the system are invariant with respect to Π. In the super-radiant phase, however, this global symmetry is broken and two new local symmetries appear, each of which describes an isolated wave function lobe, and the spectrum is doubly degenerate. This symmetry breaking, strictly only occurs in the thermodynamic limit and, at any finite j, these lobes are joined together in a total wave function that is Π invariant. That these two lobes are separated by a macroscopic amount, proportional to the square root of the system size, means that the onset of chaos is accompanied by the delocalization of the wave functions and the appearance of macroscopic coherence in the system.

Similar features occur in the three-dimensional Anderson model. This model of a disordered electron system exhibits a metal-insulator transition, in which the wave functions are localized for strong disorder and delocalized where the disorder is weak [8,59,60]. An analysis of the level statistics shows that $P(S)$ changes from Poissonian to Wigner-Dyson at the phase-transition point, which is determined by the magnitude of the random potential fluctuations. It is remarkable that our comparatively simple model should bear so many important features in common with complex disorder models, such as the Anderson model; although one feature of such models, for which we have found no evidence of in the DH, is the existence of a third universal $P(S)$ distribution precisely at the critical coupling [8].

There are two different classical limits involved with the Dicke model and, by extension, models of similar nature involving quantum spins and boson fields. First, there is the

limit of $j\to\infty$, in which the length of the spin becomes macroscopic. The second is the limit $\hbar\to 0$, which we have performed here when setting bosonic commutators equal to zero.

These limits may be applied independently and in either order. If we apply the $j\to\infty$ limit first to the DH, we obtain the effective Hamiltonians $H^{(1,2)}$. Taking then $\hbar\to 0$ by setting the commutators of the collective modes to zero, we simply obtain $H_{\rm sc}^{(1,2)}$, the two classical effective Hamiltonians. Note that the integrability of $H^{(1,2)}$ makes this ''dequantization'' direct and unambiguous. Applying this limit in the other order means that starting with the DH in the Holstein-Primakoff representation, we set $\hbar\to 0$ by setting the original field and atom bosonic commutators to zero, which results in our semiclassical Hamiltonian $H_{\rm sc}$. Subsequently, taking the $j\to\infty$ limit results in $H_{\rm sc}^{(1,2)}$ as above, showing that we obtain the same result independent of the order in which the limits are taken.

After both limits, the system described by $H_{\rm sc}^{(1,2)}$ is ''the classical'' analog of the DH, describing a macroscopic collection of atoms in terms of classical variables. This system is completely integrable, and there is no sign of chaos either in it or its quantized counterpart $H^{(1,2)}$.

These results support the recent argument put forward by Ballentine concerning the existence of so-called ''semiquantum chaos'' [61]. Semiquantum chaos is that which arises from the coupling of a quantum and a classical system, neither of which are by themselves chaotic. Ballentine studied a model of a massive particle of mass m interacting with a spin-1/2. By considering the semiclassical limit of $m\to\infty$, the semiquantum system of a quantum spin interacting with a classical particle was realized. He demonstrated that as $m\to\infty$, the chaos in the system rapidly disappeared. Our results here may be seen as the complement to this system, where the mass is kept constant but the length of the pseudospin is taken to the classical limit $j\to\infty$. Given the integrability of the DH is this limit, there is certainly no semiquantum chaos in our system, which lends additional weight to Ballentine's claim that semiquantum chaos does not exist.

The question then arises; what is the status of the two systems obtained by only taking one of the two limits. In the case of only taking the $j\to\infty$ limit, the answer is simple; $H^{(1,2)}$ is a direct quantization of $H_{\rm sc}^{(1,2)}$ and describes quantum fluctuations around classical mean fields. More interesting is the status of $H_{\rm sc}$. We have shown here that its behavior matches very closely that of the quantum DH, and that it has been derived in an almost canonical way, so its mathematical status as the semiclassical counterpart of the DH seems reasonably secure, but what is the relevance of this model to the physical system is less obvious.

The nature of the $\hbar\to 0$ limit suggests that this model might be useful in describing the model when there are a few atoms (10–20) present, and almost-classical fields, i.e., coherent states, are applied. Under these circumstances, the original DH and semiclassical model $H_{\rm sc}$ might be fruitfully compared.

ACKNOWLEDGMENTS

This work was supported by Project Nos. EPSRC GR44690/01, DFG Br1528/4-1, the WE Heraeus Foundation and the UK Quantum Circuits Network.

APPENDIX A: BOGOLIUBOV TRANSFORMATION

1. Normal phase

The two sets of bosons $\{a,b\}$ and $\{c_1,c_2\}$ may be expressed in terms of one another as

$$a^\dagger=\frac{1}{2}\left\{\frac{\cos\gamma^{(1)}}{\sqrt{\omega\varepsilon_-^{(1)}}}[(\omega+\varepsilon_-^{(1)})c_1^\dagger+(\omega-\varepsilon_-^{(1)})c_1]+\frac{\sin\gamma^{(1)}}{\sqrt{\omega\varepsilon_+^{(1)}}}[(\omega+\varepsilon_+^{(1)})c_2^\dagger+(\omega-\varepsilon_+^{(1)})c_2]\right\},$$

$$a=\frac{1}{2}\left\{\frac{\cos\gamma^{(1)}}{\sqrt{\omega\varepsilon_-^{(1)}}}[(\omega-\varepsilon_-^{(1)})c_1^\dagger+(\omega+\varepsilon_-^{(1)})c_1]+\frac{\sin\gamma^{(1)}}{\sqrt{\omega\varepsilon_+^{(1)}}}[(\omega-\varepsilon_+^{(1)})c_2^\dagger+(\omega+\varepsilon_+^{(1)})c_2]\right\},$$

$$b^\dagger=\frac{1}{2}\left\{\frac{-\sin\gamma^{(1)}}{\sqrt{\omega_0\varepsilon_-^{(1)}}}[(\omega_0+\varepsilon_-^{(1)})c_1^\dagger+(\omega_0-\varepsilon_-^{(1)})c_1]+\frac{\cos\gamma^{(1)}}{\sqrt{\omega_0\varepsilon_+^{(1)}}}[(\omega_0+\varepsilon_+^{(1)})c_2^\dagger+(\omega_0-\varepsilon_+^{(1)})c_2]\right\},$$

$$b=\frac{1}{2}\left\{\frac{-\sin\gamma^{(1)}}{\sqrt{\omega_0\varepsilon_-^{(1)}}}[(\omega_0-\varepsilon_-^{(1)})c_1^\dagger+(\omega_0+\varepsilon_-^{(1)})c_1]+\frac{\cos\gamma^{(1)}}{\sqrt{\omega_0\varepsilon_+^{(1)}}}[(\omega_0-\varepsilon_+^{(1)})c_2^\dagger+(\omega_0+\varepsilon_+^{(1)})c_2]\right\}, \quad \text{(A1)}$$

with the inverse relations

$$c_1^\dagger=\frac{1}{2}\left\{\frac{\cos\gamma^{(1)}}{\sqrt{\omega\varepsilon_-^{(1)}}}[(\varepsilon_-^{(1)}+\omega)a^\dagger+(\varepsilon_-^{(1)}-\omega)a]-\frac{\sin\gamma^{(1)}}{\sqrt{\omega_0\varepsilon_-^{(1)}}}[(\varepsilon_-^{(1)}+\omega_0)b^\dagger+(\varepsilon_-^{(1)}-\omega_0)b]\right\},$$

$$c_1=\frac{1}{2}\left\{\frac{\cos\gamma^{(1)}}{\sqrt{\omega\varepsilon_-^{(1)}}}[(\varepsilon_-^{(1)}-\omega)a^\dagger+(\varepsilon_-^{(1)}+\omega)a]-\frac{\sin\gamma^{(1)}}{\sqrt{\omega_0\varepsilon_-^{(1)}}}[(\varepsilon_-^{(1)}-\omega_0)b^\dagger+(\varepsilon_-^{(1)}+\omega_0)b]\right\},$$

$$c_2^\dagger=\frac{1}{2}\left\{\frac{\sin\gamma^{(1)}}{\sqrt{\omega\varepsilon_+^{(1)}}}[(\varepsilon_+^{(1)}+\omega)a^\dagger+(\varepsilon_+^{(1)}-\omega)a]+\frac{\cos\gamma^{(1)}}{\sqrt{\omega_0\varepsilon_+^{(1)}}}[(\varepsilon_+^{(1)}+\omega_0)b^\dagger+(\varepsilon_+^{(1)}-\omega_0)b]\right\},$$

$$c_2=\frac{1}{2}\left\{\frac{\sin\gamma^{(1)}}{\sqrt{\omega\varepsilon_+^{(1)}}}[(\varepsilon_+^{(1)}-\omega)a^\dagger+(\varepsilon_+^{(1)}+\omega)a]+\frac{\cos\gamma^{(1)}}{\sqrt{\omega_0\varepsilon_+^{(1)}}}[(\varepsilon_+^{(1)}-\omega_0)b^\dagger+(\varepsilon_+^{(1)}+\omega_0)b]\right\}. \quad \text{(A2)}$$

The angle $\gamma^{(1)}$ is the rotation angle of the coordinate system, which eliminates the interaction in the position representation, and is given by

$$\tan(2\gamma^{(1)})=\frac{4\lambda\sqrt{\omega\omega_0}}{\omega_0^2-\omega^2}. \quad \text{(A3)}$$

2. Super-radiant phase

The analogous Bogoliubov transfomations in the super-radiant phase are

$$c^\dagger=\frac{1}{2}\left\{\frac{\cos\gamma^{(2)}}{\sqrt{\omega\varepsilon_-^{(2)}}}[(\omega+\varepsilon_-^{(2)})e_1^\dagger+(\omega-\varepsilon_-^{(2)})e_1]+\frac{\sin\gamma^{(2)}}{\sqrt{\omega\varepsilon_+^{(2)}}}[(\omega+\varepsilon_+^{(2)})e_2^\dagger+(\omega-\varepsilon_+^{(2)})e_2]\right\},$$

$$c=\frac{1}{2}\left\{\frac{\cos\gamma^{(2)}}{\sqrt{\omega\varepsilon_-^{(2)}}}[(\omega-\varepsilon_-^{(2)})e_1^\dagger+(\omega+\varepsilon_-^{(2)})e_1]+\frac{\sin\gamma^{(2)}}{\sqrt{\omega\varepsilon_+^{(2)}}}[(\omega-\varepsilon_+^{(2)})e_2^\dagger+(\omega+\varepsilon_+^{(2)})e_2]\right\},$$

$$d^\dagger=\frac{1}{2}\left\{\frac{-\sin\gamma^{(2)}}{\sqrt{\tilde{\omega}\varepsilon_-^{(2)}}}[(\tilde{\omega}+\varepsilon_-^{(2)})e_1^\dagger+(\tilde{\omega}-\varepsilon_-^{(2)})e_1]+\frac{\cos\gamma^{(2)}}{\sqrt{\tilde{\omega}\varepsilon_+^{(2)}}}[(\tilde{\omega}+\varepsilon_+^{(2)})e_2^\dagger+(\tilde{\omega}-\varepsilon_+^{(2)})e_2]\right\},$$

$$d=\frac{1}{2}\left\{\frac{-\sin\gamma^{(2)}}{\sqrt{\tilde{\omega}\varepsilon_-^{(2)}}}[(\tilde{\omega}-\varepsilon_-^{(2)})e_1^\dagger+(\tilde{\omega}+\varepsilon_-^{(2)})e_1]+\frac{\cos\gamma^{(2)}}{\sqrt{\tilde{\omega}\varepsilon_+^{(2)}}}[(\tilde{\omega}-\varepsilon_+^{(2)})e_2^\dagger+(\tilde{\omega}+\varepsilon_+^{(2)})e_2]\right\}; \quad \text{(A4)}$$

and

$$e_1^\dagger=\frac{1}{2}\left\{\frac{\cos\gamma^{(2)}}{\sqrt{\omega\varepsilon_-^{(2)}}}[(\varepsilon_-^{(2)}+\omega)c^\dagger+(\varepsilon_-^{(2)}-\omega)c]-\frac{\sin\gamma^{(2)}}{\sqrt{\tilde{\omega}\varepsilon_-^{(2)}}}[(\varepsilon_-^{(2)}+\tilde{\omega})d^\dagger+(\varepsilon_-^{(2)}-\tilde{\omega})d]\right\},$$

$$e_1=\frac{1}{2}\left\{\frac{\cos\gamma^{(2)}}{\sqrt{\omega\varepsilon_-^{(2)}}}[(\varepsilon_-^{(2)}-\omega)c^\dagger+(\varepsilon_-^{(2)}+\omega)c]-\frac{\sin\gamma^{(2)}}{\sqrt{\tilde{\omega}\varepsilon_-^{(2)}}}[(\varepsilon_-^{(2)}-\tilde{\omega})d^\dagger+(\varepsilon_-^{(2)}+\tilde{\omega})d]\right\},$$

$$e_2^\dagger=\frac{1}{2}\left\{\frac{\sin\gamma^{(2)}}{\sqrt{\omega\varepsilon_+^{(2)}}}[(\varepsilon_+^{(2)}+\omega)c^\dagger+(\varepsilon_+^{(2)}-\omega)c]+\frac{\cos\gamma^{(2)}}{\sqrt{\tilde{\omega}\varepsilon_+^{(2)}}}[(\varepsilon_+^{(2)}+\tilde{\omega})d^\dagger+(\varepsilon_+^{(2)}-\tilde{\omega})d]\right\},$$

$$e_2=\frac{1}{2}\left\{\frac{\sin\gamma^{(2)}}{\sqrt{\omega\varepsilon_+^{(2)}}}[(\varepsilon_+^{(2)}-\omega)c^\dagger+(\varepsilon_+^{(2)}+\omega)c]+\frac{\cos\gamma^{(2)}}{\sqrt{\tilde{\omega}\varepsilon_+^{(2)}}}[(\varepsilon_+^{(2)}-\tilde{\omega})d^\dagger+(\varepsilon_+^{(2)}+\tilde{\omega})d]\right\}, \quad \text{(A5)}$$

where the angle $\gamma^{(2)}$ is given by

$$\tan(2\gamma^{(2)})=\frac{2\omega\omega_0\mu^2}{\omega_0^2-\mu^2\omega^2} \quad \text{(A6)}$$

and where

$$\tilde{\omega}\equiv\frac{\omega_0}{2}\left(1+\frac{\lambda^2}{\lambda_c^2}\right). \quad \text{(A7)}$$

APPENDIX B: SQUEEZING VARIANCES

The preceding Bogoliubov transformations may be used to derive exact expressions for the squeezing variances of the ground-state wave function in the thermodynamic limit, as discussed in Sec. III. In the normal phase, they are given by

$$(\Delta x)^2=\frac{1}{2\omega}\left(1+\frac{\varepsilon_+^{(1)}(\omega-\varepsilon_-^{(1)})\cos^2\gamma^{(1)}+\varepsilon_-^{(1)}(\omega-\varepsilon_+^{(1)})\sin^2\gamma^{(1)}}{\varepsilon_-^{(1)}\varepsilon_+^{(1)}}\right),$$

$$(\Delta p_x)^2=\frac{\omega}{2}\left(1+\frac{(\varepsilon_-^{(1)}-\omega)\cos^2\gamma^{(1)}+(\varepsilon_+^{(1)}-\omega)\sin^2\gamma^{(1)}}{\omega}\right), \quad \text{(B1)}$$

$$(\Delta y)^2=\frac{1}{2\omega_0}\left(1+\frac{\varepsilon_+^{(1)}(\omega_0-\varepsilon_-^{(1)})\sin^2\gamma^{(1)}+\varepsilon_-^{(1)}(\omega_0-\varepsilon_+^{(1)})\cos^2\gamma^{(1)}}{\varepsilon_-^{(1)}\varepsilon_+^{(1)}}\right),$$

$$(\Delta p_y)^2=\frac{\omega_0}{2}\left(1+\frac{(\varepsilon_-^{(1)}-\omega_0)\sin^2\gamma^{(1)}+(\varepsilon_+^{(1)}-\omega_0)\cos^2\gamma^{(1)}}{\omega_0}\right), \tag{B2}$$

whereas in the super-radiant phase we find

$$(\Delta x)^2=\frac{1}{2\omega}\left(1+\frac{\varepsilon_+^{(2)}(\omega-\varepsilon_-^{(2)})\cos^2\gamma^{(2)}+\varepsilon_-^{(2)}(\omega-\varepsilon_+^{(2)})\sin^2\gamma^{(2)}}{\varepsilon_-^{(2)}\varepsilon_+^{(2)}}\right),$$

$$(\Delta p_x)^2=\frac{\omega}{2}\left(1+\frac{(\varepsilon_-^{(2)}-\omega)\cos^2\gamma^{(2)}+(\varepsilon_+^{(2)}-\omega)\sin^2\gamma^{(2)}}{\omega}\right), \tag{B3}$$

$$(\Delta y)^2=\frac{1}{2\omega_0}\left(1+\frac{\varepsilon_+^{(2)}(\tilde{\omega}-\varepsilon_-^{(2)})\sin^2\gamma^{(2)}+\varepsilon_-^{(2)}(\tilde{\omega}-\varepsilon_+^{(2)})\cos^2\gamma^{(2)}}{\varepsilon_-^{(2)}\varepsilon_+^{(2)}}\right),$$

$$(\Delta p_y)^2=\frac{\omega_0}{2}\left(1+\frac{(\varepsilon_-^{(2)}-\tilde{\omega})\sin^2\gamma^{(2)}+(\varepsilon_+^{(2)}-\tilde{\omega})\cos^2\gamma^{(2)}}{\tilde{\omega}}\right). \tag{B4}$$

These results are plotted in the main body of the text.

[1] R.C. Hilborn, *Chaos and Nonlinear Dynamics* (Oxford University Press, Oxford, 2000).
[2] M.C. Gutzwiller, *Chaos in Classical and Quantum Mechanics* (Springer, Berlin, 1990).
[3] F. Haake, *Quantum Signatures of Chaos* (Springer, Berlin, 2001).
[4] M.V. Berry and M. Tabor, Proc. R. Soc. London, Ser. A **356**, 375 (1977).
[5] O. Bohigas, M.J. Giannoni, and C. Schmidt, Phys. Rev. Lett. **52**, 1 (1984).
[6] P. Pechukas, Phys. Rev. Lett. **51**, 943 (1983); T. Yukawa, *ibid.* **54**, 1883 (1985).
[7] A. Peres, Phys. Rev. A **30**, 1610 (1984); R. Schack and C.M. Caves, Phys. Rev. Lett. **71**, 525 (1993); Phys. Rev. E **53**, 3257 (1996); **53**, 3387 (1996).
[8] I.K. Zharekeshev and B. Kramer, Phys. Rev. B **51**, 17 239 (1995); Phys. Rev. Lett. **79**, 717 (1997).
[9] Ph. Jacquod and D.L. Shepelyansky, Phys. Rev. Lett. **79**, 1837 (1997).
[10] B. Georgeot and D.L. Shepelyansky, Phys. Rev. Lett. **81**, 5129 (1998).
[11] B. Georgeot and D.L. Shepelyansky, Phys. Rev. E **62**, 3504 (2000); **62**, 6366 (2000).
[12] D. Delande and J.C. Gay, Phys. Rev. Lett. **57**, 2006 (1986).
[13] Th. Zimmermann, H.-D. Meyer, H. Köppel, and L.S. Cederbaum, Phys. Rev. A **33**, 4334 (1986).
[14] G. Montambaux, D. Poilblanc, J. Bellissard, and C. Sire, Phys. Rev. Lett. **70**, 497 (1993).
[15] Y. Alhassid and N. Whelan, Phys. Rev. Lett. **67**, 816 (1991).
[16] J. Zakrzewski and M. Kuś, Phys. Rev. Lett. **67**, 2749 (1991).
[17] L. Junqing, L. Fang, X. YongZhong, Z. Wei, and W.D. Heiss, Phys. Rev. E **65**, 047203 (2002).
[18] S. Sachdev, *Quantum Phase Transitions* (Cambridge University Press, Cambridge, 1999).
[19] W.D. Heiss and S. Radu, Phys. Rev. E **52**, 4762 (1995); W.D. Heiss and A.A. Kotzé, Phys. Rev. A **44**, 2403 (1991).
[20] W.D. Heiss and Müller, Phys. Rev. E **66**, 016217 (2002); W.D. Heiss and A.L. Sannino, Phys. Rev. A **43**, 4159 (1991); W.D. Heiss, M. Müller, and I. Rotter, Phys. Rev. E **58**, 2894 (1998).
[21] R.H. Dicke, Phys. Rev. **93**, 99 (1954).
[22] A.V. Andreev, V.J. Emel'yanov, and Yu.A. Il'inskii, *Cooperative Effects in Optics* (IOP, Bristol, 1993).
[23] M.G. Benedict, *et al.*, *Super-Radiance* (IOP, Bristol, 1996).
[24] C. Emary and T. Brandes, Phys. Rev. Lett. **90**, 044101 (2003).
[25] K. Hepp and E.H. Lieb, Ann. Phys. (N.Y.) **76**, 360 (1973).
[26] Y.K. Wang and F.T. Hioe, Phys. Rev. A **7**, 831 (1973).
[27] K. Hepp and E.H. Lieb, Phys. Rev. A **8**, 2517 (1973).
[28] G. Cromer Duncan, Phys. Rev. A **9**, 418 (1974).
[29] T. Holstein and H. Primakoff, Phys. Rev. **58**, 1098 (1949).
[30] E. Ressayre and A. Tallet, Phys. Rev. A **11**, 981 (1975); F. Persico and G. Vetri, *ibid.* **12**, 2083 (1975).
[31] M. Hillery and L.D. Mlodinow, Phys. Rev. A **31**, 797 (1984).
[32] R. Graham and M. Höhnerbach, Z. Phys. B: Condens. Matter **57**, 233 (1984); Phys. Lett. **101A**, 61 (1984).
[33] R. Graham and M. Höhnerbach, Phys. Rev. Lett. **57**, 1378 (1986).
[34] C.H. Lewenkopf, M.C. Nemes, V. Marvulle, M.P. Pato, and W.F. Wrenszinski, Phys. Lett. A **155**, 113 (1991).
[35] M. Kuś, Phys. Rev. Lett. **54**, 1343 (1985).
[36] K. Furuya, M.C. Nemes, and G.Q. Pellegrino, Phys. Rev. Lett. **80**, 5524 (1998); R.M. Angelo, K. Furuya, M.C. Nemes, and G.Q. Pellegrino, Phys. Rev. A **64**, 043801 (2001).

[37] P.W. Milonni, J.R. Ackerhalt, and H.W. Galbraith, Phys. Rev. Lett. **50**, 966 (1983).
[38] L. Müller, J. Stolze, H. Leschke, and P. Nagel, Phys. Rev. A **44**, 1022 (1991).
[39] G.A. Finney and J. Gea-Banacloche, Phys. Rev. A **50**, 2040 (1994); Phys. Rev. E **54**, 1449 (1996).
[40] F.T. Arrechi, E. Courtens, R. Gilmore, and H. Thomas, Phys. Rev. A **6**, 2211 (1972).
[41] X. Wang and K. Mølmer, Eur. Phys. J. D **18**, 385 (2002).
[42] R.F. Bishop and A. Vourdas, Phys. Rev. A **50**, 4488 (1994).
[43] P.R. Eastham and P.B. Littlewood, Phys. Rev. B **64**, 235101 (2001).
[44] R. Glauber, Phys. Rev. **131**, 2766 (1963).
[45] D. Walls and G.J. Milburn, *Quantum Optics* (Springer, Berlin, 1995).
[46] D.F. Walls and P. Zoller, Phys. Rev. Lett. **47**, 709 (1981).
[47] H. Saiko and M. Ueda, Phys. Rev. A **59**, 3959 (1999).
[48] R.F. Bishop and A. Vourdas, J. Phys. A **19**, 2525 (1986).
[49] T. Guhr, A. Müller-Groeling, and H.A. Weidenmüller, Phys. Rep. **299**, 189 (1998).
[50] G. Casati, B.V. Chirikov, and I. Guarneri, Phys. Rev. Lett. **54**, 1350 (1985).
[51] H. Wu, M. Vallières, D.H. Feng, and D.W.L. Sprung, Phys. Rev. A **42**, 1027 (1990).
[52] B.R. Judd, J. Chem. Phys. **67**, 1174 (1977); J. Phys. C **12**, 1685 (1979).
[53] R.F. Bishop and C. Emary, J. Phys. A **34**, 5635 (2001).
[54] I.I. Rabi, Phys. Rev. **51**, 652 (1937).
[55] I.C. Percival, J. Phys. B **6**, L229 (1973).
[56] J.P. Paz and W.H. Zurek, in *Environment-Induced Decoherence and the Transition From Quantum to Classical*, Proceedings of the Les Houches Summer School, Session 72, edited by R. Kaiser, C. Westbrook, and F. David (Springer, Berlin, 2001).
[57] H. Goldstein, C.P. Poole, and J.L. Safko, *Classical Mechanics*, 3rd ed. (Addison-Wesley, New York, 2001).
[58] L.M. Narducci, M. Orszag, and R.A. Tuft, Phys. Rev. A **8**, 1892 (1973).
[59] For a review, see P.A. Lee and T.V. Ramakrishnan, Rev. Mod. Phys. **57**, 287 (1985).
[60] S. Fishman, D.R. Grempel, and R.E. Prange, Phys. Rev. Lett. **49**, 509 (1982); Phys. Rev. A **29**, 1639 (1984); R.E. Prange in *Quantum Chaos*, edited by H.A. Cerdeira, R. Ramaswamy, M.C. Gutzwiller, and G. Casati (World Scientific, Singapore, 1991).
[61] L.E. Ballentine, Phys. Rev. E **63**, 056204 (2001).